OPTICAL POLARIMETRY OF FIVE STARS

by

MICHAEL JOHN ECCLES

B.Eng., Liverpool University, 1965

Ph.D., Liverpool University, 1969

A THESIS SUBMITTED IN PARTIAL FULFILLMENT

OF THE REQUIREMENTS FOR THE DEGREE OF

MASTER OF SCIENCE

in the Department of Physics

We accept this thesis as conforming

to the required standard

[redacted]

J.L. Climenhaga

[redacted]

F.D.A. Hartwick

[redacted]

G.G. Miller

[redacted]

J.B. Tatum

[redacted]

J.T. Weaver

UNIVERSITY OF VICTORIA
OCTOBER 1978

ABSTRACT

Supervisor: Dr. J. L. Climenhaga

This thesis describes a new solid state optical polarimeter and the observations of five stars made with it. Three of the stars, Rho Cassiopeiae, 89 Herculis and HD 217476, are supergiants which appear to be losing mass. It has been suggested that these stars may be binaries with long periods. A monitoring of the linearly polarized light from the three stars has not, however, shown the characteristic polarimetric signature of binary motion.

A polarimetric study of Beta Lyrae in the red and near infra-red part of the spectrum shows an increase in polarization at primary eclipse greater than that previously reported for shorter wavelengths. It is suggested that the polarized flux at long wavelengths is produced further out in the binary envelope than is the short wavelength flux.

The polarization of Algol has been studied throughout several orbital cycles and remains always less than 0.2%. This is in good agreement with the recent work of Rudy and Kemp.

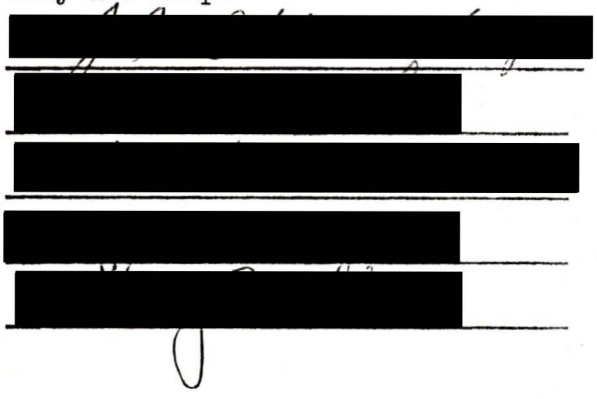

TABLE OF CONTENTS

LIST OF TABLES

LIST OF FIGURES

ACKNOWLEDGEMENTS

I wish to acknowledge the help and support of my supervisor, Dr. J.L. Climenhaga, throughout the course of this work. I wish to similarly thank the other members of my graduate advisory committee.

I further wish to acknowledge the help of many members of the staff and faculty of the Department of Physics. In particular, I thank Jim Stilburn for help with the polarimeter optics, Dave Balam for sharing many a long, cold observing run, Dr. C.D. Scarfe for explaining the geometry of binary star systems, Dr. J.A. Burke for help in understanding the Davis-Greenstein mechanism, and the department mechanical workshop for fabricating the polarimeter head.

On a more personal note, I will always remember the friendly companionship and help of the other graduate astronomy students. The support and encouragement of my wife, Pam, (and son, Mark) during the past two years has been of inestimable value.

Finally I acknowledge with thanks the financial support of the university in the form of University of Victoria Fellowships for the years 1976-7 and 1977-8.

DEDICATION

I dedicate this thesis to my parents with grateful thanks for their many sacrifices.

CHAPTER 1. INTRODUCTION

Electromagnetic radiation is completely described by three parameters, intensity, frequency and state of polarization. Our knowledge of celestial bodies outside the solar system has been almost entirely gained through the first two parameters and it is only fairly recently that the state of polarization has been considered. The general existence of polarized light has been known since the 17th century and the polarization of skylight since the early 19th century, but the present day interest in astronomical sources of polarized light can be said to have started in 1946 with the work of Chandrasekhar (1946). He incorporated anisotropic scattering into the equation of radiative transfer and, for the case of opacity due to electron scattering, obtained the result that the light at the limb of a spherical star would show a net linear polarization of 11%, the electric vector being tangential to the limb. Subsequent work has shown this estimate to be too large, but in any case the integrated light over the whole disk of the star would be non-polarized. Only if there were some departure from spherical symmetry, such as a circumstellar disk, or if part of the limb were eclipsed, would any polarization actually be observed.

Chandrasekhar's work prompted both Hall (1949) and Hiltner (1949) to look for variable polarization in known binary stars. They did not find any variability but did make the rather remarkable discovery that most stars near the galactic plane are linearly polarized to a few percent, and they suggested that the effect was interstellar in origin. The Davis-Greenstein

(1951) explanation of this polarization through selective absorption of rotating dust grains aligned along the interstellar magnetic field lines is now generally accepted, although Purcell (1975) has pointed out that the required magnetic field is too high.

The first reproducible polarization changes attributable to binary motion were observed by Shakhovskoi (1962) for the Beta Lyrae system. The intrinsic nature of the variable polarization was shown by the correlation with photometric observations. Since 1962 several other systems have been found to show variable intrinsic polarization. The polarization mechanism most favoured is electron scattering in a circumstellar envelope or disk.

The intrinsic polarization of an isolated star is very difficult to measure because of the presence of the usually much greater interstellar component. However interstellar polarization is constant over a period of many years and has a well defined variation with wavelength. Thus the intrinsic polarization of certain supergiant stars has been detected through either short term amplitude changes or spectral differences in the overall observed polarization. Furthermore, late type supergiants should have a polarization spectrum given by scattering from a combination of molecules, electrons, and grains, quite different from that of interstellar polarization.

Apart from studying the interstellar magnetic field, stellar polarization data have been primarily used to estimate the amount of scattering material

in a particular system, and, in the case of binary stars, to give information on their spatial orientation.

The present investigation has been concerned with polarimetric observations of two classes of objects. The first class comprises three late type supergiant stars, 89 Herculis, Rho Cassiopeiae and HD 217476, which are suspected by Smolinski (1977) of being binary stars even though standard photometric and spectroscopic tests do not support this idea. Smolinski gives as evidence observations of mass loss, emission lines and composite energy distributions. If the three stars were binary and also undergoing mass exchange, a periodic variation in linear polarization might well be seen, although it would be superimposed on the interstellar background.

The second class comprises two well known binary stars, Algol and Beta Lyrae. At the time this research commenced (May 1977), there were no polarimetric data published for Algol, which was surprising considering the brightness of the system and the mass transfer known to be taking place. The binary star Beta Lyrae has been extensively observed in the visible spectrum but not in the red part of the spectrum possible with the present polarimeter. A comparison of polarimetric data for the two spectral regions may suggest a possible scattering mechanism.

Astronomical polarimetry has only recently become practical owing to the difficulty of constructing a polarimeter which has an intrinsic polarization of less than a few tenths of a percent and which has good

sensitivity and repeatability. Part of this investigation has been the study of previously built polarimeters followed by the design and construction of a new type of polarimeter dispensing with the usual photomultiplier tube in favour of a silicon diode detector. Although the silicon diode is electrically noisier and thus less sensitive than the photomultiplier tube, it is robust, highly linear, virtually insensitive to the state of polarization of the incident radiation and very compact. The last two points have made possible the construction of a lightweight polarimeter for use on the 31 cm telescope at the University of Victoria. All the results described below have been made with this polarimeter at Victoria, with the exception of those taken on JD 2443395 when the 41 cm telescope of the Dominion Astrophysical Observatory on Mt. Kobau, B.C., was used.

Before considering the observational data for the two classes of objects mentioned above, it is necessary to give the theoretical background to the various mechanisms capable of producing polarized radiation, and then to examine the performance of the polarimeter. Only then can the true significance of the results be determined. For these reasons, the next chapter is concerned with the theoretical production of polarization, and is followed by a description of the present polarimeter. The observations are then presented in Chapter 4 and discussed in Chapter 5.

CHAPTER 2. ASTRONOMICAL SOURCES OF POLARIZATION

The principal processes, both intrinsic and extrinsic to a stellar system, which cause the starlight to be polarized will now be considered.

2.1. Interstellar polarization

Hall (1949) and Hiltner (1949) found that many stars near the galactic plane are linearly polarized. Their data and those of more recent investigators (Serkowski, Mathewson and Ford, 1975) show three striking characteristics which strongly suggest an interstellar origin for the polarization.

(i) In general, the vectors representing the polarization of different stars show approximate parallelism for small galactic latitudes over a considerable range of galactic longitude. This is seen best in the survey of 1800 stars by Mathewson and Ford (1970). Figure 2.1 shows only a general correlation of directions and not complete alignment.

(ii) There is a correlation between polarization and interstellar reddening such that the ratio of polarization to colour excess has a maximum value. Figure 2.2, taken from Hiltner (1956b), shows this relationship for the Cassiopeia region where, expressing both the polarization, P_m, and colour excess, E_{B-V}, in magnitudes (i.e., $P_m = 2.5 \log[I \text{ max} / I \text{ min}]$), the observations fit the relationship

$$\frac{P_m}{E_{B-V}} \leqslant 0.18 \qquad (1)$$

This observation alone strongly points to clouds of interstellar dust, not always completely aligned, being responsible for the polarization.

(iii) The variation of polarization with wavelength is similar for all stars so far observed and, furthermore, fits the Davis-Greenstein (1951) model described below. Figure 2.3, from Coyne (1974), shows the fit of multicolour polarimetric observations to model calculations. The maximum polarization occurs at a wavelength close to the mean particle radius of 0.4 microns used in the model.

The polarization spectral curve is quite different from the extinction spectral curve in that the extinction continues to rise at ever shorter wavelengths whereas the polarization reaches a maximum at about 0.55 micron and then falls with decreasing wavelength. A comparison of figures 2.3 and 2.4, both from Coyne (1974), shows this effect. The reason is that a non-spherical dust grain causes polarization through the longer axis absorbing or scattering more light than the shorter axes, and hence preferentially weakening one orthogonal component of the incident light. Only when the grain size is comparable to the incident wavelength will there be this preferential weakening. If the grain is too small, the light will be unaffected and if too large, both orthogonal components

will be effectively absorbed or scattered to the same extent.

The existence of large scale parallelism requires a large scale aligning field, which was originally suggested by Davis and Greenstein (1951) to be the interstellar magnetic field. Their theory of grain alignment has stood the test of time and will now be considered.

2.1.1 The Davis-Greenstein theory

This theory provides a mechanism for aligning elongated dust grains in spite of the tendency towards rapid spin from collisions with interstellar hydrogen. In the absence of any aligning torque, the orientation of the grains will be completely random, and, by the equipartition theorem, their mean kinetic energy of rotation will be equal to the mean kinetic energy of the interstellar gas*. For the grains to be aligned, any torque must be dissipative, otherwise the grains will simply precess and the average orientation will remain random. Davis and Greenstein suggest that paramagnetic absorption, the magnetic equivalent of dielectric loss, causes the magnetization of the rotating dust grain to lag behind the interstellar magnetic field such that the grain is eventually ($\sim 10^{13}$ seconds) aligned with this magnetic field.

The magnetic properties of many substances are such that if the substance is put in a magnetic field, $\underline{B}$, which varies with time according to

$$\underline{B} = \hat{e} B_o \cos \omega t, \qquad (2)$$

*provided the gas is monatomic.

where $\hat{e}$ is a fixed unit vector in the $\underline{B}$ direction, the magnetization will be given by

$$\underline{M} = \hat{e} B_o [\chi' \cos\omega t + \chi'' \sin\omega t], \qquad (3)$$

χ' and χ'' are the real and imaginary parts of the complex susceptibility. The amount of heat generated by the alternating magnetic field is determined by χ'', and this absorption of energy is called paramagnetic absorption.

Considering Figure 2.5, the magnetic field $\underline{B}$ is fixed in space, and the dust grain rotates with angular velocity, $\underline{\omega}$, about an axis initially fixed in space. The following analysis will show that one effect of the magnetic field is to cause precession, such that the axis of rotation of the grain moves in space.

Let $\hat{x}$, $\hat{y}$ and $\hat{z}$ be unit vectors in the coordinate system fixed in space, and $\hat{i}$, $\hat{j}$, and $\hat{k}$ be unit vectors in the coordinate system of the dust grain. Chose the origin of time so that

$$\hat{x} = \hat{i}\cos\omega t - \hat{j}\sin\omega t, \quad \hat{y} = \hat{i}\sin\omega t + \hat{j}\cos\omega t, \quad \hat{z} = \hat{k} = \frac{\underline{\omega}}{\omega} \qquad (4)$$

From 2.5 (a), a stationary observer sees $\underline{B}$ confined to the xz plane so that

$$\underline{B} = B_x\hat{x} + B_z\hat{z} \qquad (5)$$

From the point of view of an observer rotating with the dust grain,

$$\underline{B} = B_z\hat{k} + B_x[\hat{i}\cos\omega t - \hat{j}\sin\omega t] \qquad (6)$$

Hence the magnetization seen by the rotating dust grain is

$$\underline{M} = \chi_o B_z \hat{k} + B_x [\hat{i}(\chi' \cos\omega t + \chi'' \sin\omega t) + \hat{j}(-\chi' \sin\omega t + \chi'' \cos\omega t)] \quad (7)$$

or

$$\underline{M} = \chi_o B_z \hat{z} + \chi' B_x \hat{x} + \chi'' B_x \hat{y} \quad (8)$$

where χ_o is the static susceptibility.

When $\omega = o$, then $\chi'' = o$ and $\chi_o = \chi'$.

The $\hat{z}$ component of the magnetization has no effect on the rotation, the $\hat{x}$ component causes the precession mentioned above, and only the $\hat{y}$ component causes a change in the magnitude of $\underline{\omega}$, through the dissipative χ'' term.

Hence, the dissipative term can be written

$$\underline{M}_d = \chi'' B_x \hat{y} = \chi''(\underline{\omega} \times \underline{B})/\omega . \quad (9)$$

Or, if V is the volume of the grain, its magnetic moment is $V\underline{M}_d$, and the torque acting on this dipole is

$$\underline{T} = V\underline{M}_d \times \underline{B} = V \chi'' \omega^{-1}(\underline{\omega} \times \underline{B}) \times \underline{B}. \quad (10)$$

Considering figure 2.5(b), $\underline{L}$ is the total angular momentum vector and the dust grain spins about the axis OA such that its instantaneous angular velocity, $\underline{\omega}$, is the vector sum of the rotations about $\underline{L}$ and OA, its average over one cycle being $\underline{\omega}_{av}$.

Now,

$$\frac{d\underline{L}}{dt} = \underline{T} = V \chi'' \omega^{-1}(\underline{\omega} \times \underline{B}) \times \underline{B} \quad (11)$$

and as the average angular velocity is parallel to $\underline{L}$, the average torque acting on the grain lies in the plane of $\underline{L}$ and $\underline{B}$, and is normal to $\underline{B}$. Hence $\underline{L}$ tends to approach $\underline{B}$, its tip moving along the dotted line of figure 2.5(b), so that eventually $\underline{L}$ is parallel to $\underline{B}$, and the dust grain is aligned with the interstellar magnetic field. To determine which axis is the rotation axis, consider the rate of change of energy, E,

$$\frac{dE}{dt} = \underline{T}.\underline{\omega} = -V \chi'' \omega^{-1} (\underline{\omega} \times \underline{B})^2. \qquad (12)$$

As is usually the case, this means that the energy will decrease to a minimum when $\underline{\omega}$ is as nearly parallel to $\underline{B}$ as possible. Now for a body with a moment of inertia, I, the ratio of energy to angular momentum is

$$\frac{E}{|\underline{L}|} = \frac{1}{2} I \omega^2 / |I \underline{\omega}| = \left| \frac{\underline{\omega}}{2} \right| \qquad (13)$$

and so, for an isolated grain with constant angular momentum, minimum energy corresponds to minimum angular velocity. This occurs with rotation about the shortest axis.

Thus the Davis-Greenstein mechanism predicts that the dust grains will rotate with their shortest axis aligned with the interstellar magnetic field. The component of light with electric vector normal to the short axis of the grain will be scattered or absorbed more than the orthogonal component and hence the light will be linearly polarized such that the electric vector is parallel to the magnetic field.

Purcell (1975) has criticised this mechanism on the grounds that it requires an interstellar magnetic field of 10^{-9} - 10^{-8} tesla for complete

alignment, whereas other measurements (Faraday depolarization of radio waves) suggest 10^{-10} tesla. The rate of rotation of the dust grains is not known, and this will have a direct influence on the relaxation time for complete alignment. However, it is still believed that the Davis-Greenstein model is basically correct.

2.2 Circumstellar polarization

A number of linearly polarized stars exhibit time variability, which has been attributed to changes in a non spherical circumstellar envelope. The changes could be in the density of the envelope or, for the case of a binary star, in the physical orientation of the envelope with respect to the observer. Theoretical models capable of explaining this variability will now be considered; but first the four Stokes parameters will be discussed.

2.2.1 The Stokes parameters

It may seem convenient to refer to linear polarization in terms of the percentage polarization and the orientation of the plane of vibration of the electric vector. However, for theoretical purposes, and to a lesser extent, for analytical purposes, it has been found more convenient to describe polarization in terms of the Stokes parameters, I, Q, U and V. The total intensity of the light is given by I, the amount and orientation of linear polarization by a combination of Q and U, and the amount and handedness of circular polarization by V. The parameters are defined in terms of observable quantities as follows.

Suppose there exists a rotatable linear polarization analyzer (e.g. a sheet of polaroid) which can be rotated transversely to a 100% linearly polarized beam of light. If the maximum transmitted light occurs with the transmission axis of the polaroid vertical, then Q is equal to +1

and if the maximum occurs with the polarizer horizontal, Q is -1. A maximum with the analyzer at 45° in the first quandrant corresponds to U equal to +1 and at 45° in the second quadrant to U equal to -1. In this case there is no circular component and V equals zero.

If, however, the beam were completely circularly polarized, V would be equal to either +1 for right handedness or -1 for left handedness. Here Q and U would be zero.

Alternatively, the Stokes parameters can be defined in terms of the orthogonal components into which any light ray can be resolved. Letting E_A represent the vertical and E_B the horizontal electric field strength, and letting δ represent their phase difference, then

$$I = \langle E_A^2 \rangle + \langle E_B^2 \rangle \tag{14}$$

$$U = \langle E_A^2 \rangle - \langle E_B^2 \rangle \tag{15}$$

$$Q = 2 \langle E_A E_B \rangle \cos \delta \tag{16}$$

$$V = 2 \langle E_A E_B \rangle \sin \delta \tag{17}$$

where $\langle \rangle$ indicates time averaging. The present polarimeter cannot measure circular polarization, and so for the remainder of this thesis, δ will be taken as zero and only linear polarization considered. The linear polarization, p, is now defined as

$$p = \frac{Imax - Imin}{Imax + Imin} \tag{18}$$

where I max, I min are the maximum and mimimum intensities observed when

the polaroid analyzer is rotated transversely to the beam of light.

In terms of the Stokes parameters, p is written

$$p = \frac{\sqrt{Q^2 + U^2}}{I} . \qquad (19)$$

(Note that this p is different from the p_m defined earlier in section 2.1)

The polarization angle, θ, is defined by

$$\theta = \tfrac{1}{2} \tan^{-1}\left(\frac{U}{Q}\right) \qquad (20)$$

and usually measured from north going east.

2.2.2 Scattering in a uniform circumstellar disk

The first attempt at predicting the polarization due to scattering in a circumstellar envelope was by Shakhovskoi (1965), who took the idealised case of a uniform circumstellar disk of constant mean radius surrounding the brighter member of an eclipsing binary system.

The observed polarization of the system is

$$p = p_{disk} . \frac{\Phi_{disk}}{l . \Phi_o} \qquad (21)$$

where p_{disk} is the intrinsic polarization of the disk,

Φ_{disk} is the scattered flux from the disk,

Φ_o is the total flux of the system outside eclipse,

and l is the relative brightness of the system during eclipse.

Outside of eclipse, the observed polarization is a constant and equal to

$$p_o \doteq p_{disk} \cdot \frac{\Phi_{disk}}{\Phi_o} \quad . \tag{22}$$

Shakhovskoi showed how the ratio p_o / p_{disk} leads to an estimate of the scattering mass, as follows.

For early type stars, assuming the dominant scattering mechanism to be first order electron scattering,

$$\Phi_{disk} = \sigma \cdot N_e \cdot F_* \cdot W \tag{23}$$

where N_e is the total number of electrons in the disk,

F_* is the flux density of the central star,

and W is the dilution factor at the disk mean radius.

Rearranging and substituting for F_* and Φ_{disk}, the number of electrons is equal to

$$N_e = \frac{\pi R_*^2}{\sigma W} \cdot \frac{p_o}{p_{disk}} \tag{24}$$

R_* being the radius of the central star.

The mass of the disk can then be estimated if the ionic species are known. For a later spectral class star, where atoms, molecules and dust particles may all be present, the picture is not so clear. However, an estimate of the mass can still be made if the approximate temperature and pressure of the disk are known.

To compute the disk polarization, p_{disk}, consider figure 2.6(a) in which

radiation from the central star is scattered off a small volume element at position, α , through a scattering angle, Ψ . The position angle, α , is measured from the line OA which is in the plane containing the stellar angular momentum and the earth, $\oplus$. The disk is considered to be made up of infinitesimally thin rings. The polarization of each ring can be easily calculated, and a summation over all the rings gives the net disk polarization. The angles, i and ϕ , are the inclination of the orbital plane to the tangent plane of the sky and inclination of the scattering plane to the orbital plane, respectively.

The scattered fluxes, having electric vectors parallel with and perpendicular to the scattering plane are

$$\Phi_y = \sigma \, ne \cos^2\Psi \, I_* \, d\omega \qquad (25)$$

$$\Phi_x = \sigma \, ne \, I_* \, d\omega \qquad (26)$$

where ne is the number of electrons in the volume element,

$d\omega$ is the solid angle subtended by the volume element at the central star,

I_* is the specific intensity of the central star,

and σ is the scattering cross-section for free electrons.

For a uniform circular ring, σ ne I_* $d\omega$ is a constant, K, say, thus

$$\Phi_x = K \quad \text{and} \quad \Phi_y = K \cos^2\Psi \, . \qquad (27)$$

Considering figure 2.6(b) and taking the reference axes to be normal to

and in the plane of the disk, the orthogonal electric field strengths of the scattered radiation can be written

$$E_{xo} = E_x \sin\phi - E_y \cos\phi \tag{28}$$

$$E_{yo} = E_x \cos\phi + E_y \sin\phi \tag{29}$$

and thus the Stokes parameters, referred to the disk's coordinate system, are

$$\begin{aligned} I &= \langle E_{yo}^2 \rangle + \langle E_{xo}^2 \rangle \\ &= E_x^2 + E_y^2 \end{aligned} \tag{30}$$

$$\begin{aligned} Q &= \langle E_{yo}^2 \rangle - \langle E_{xo}^2 \rangle \\ &= (E_x^2 - E_y^2)\cos 2\phi \end{aligned} \tag{31}$$

$$\begin{aligned} U &= 2\langle E_{yo} E_{xo} \rangle \\ &= (E_x^2 - E_y^2)\sin 2\phi \end{aligned} \tag{32}$$

where use has been made of the fact that $\langle E_x E_y \rangle$ is zero.

Now, the flux is proportional to the square of the electric field strength. As only the ratios of Stokes parameters are actually observable, the constant of proportionality can be set equal to unity and the parameters redefined as

$$I = \Phi_x + \Phi_y \tag{33}$$

$$Q = (\Phi_x - \Phi_y)\cos 2\phi \tag{34}$$

and

$$U = (\Phi_x - \Phi_y)\sin 2\phi \tag{35}$$

or, using equation (27),

$$I = K(1 + \cos^2\psi) \tag{36}$$

$$Q = K \sin^2\Psi \cos 2\phi \tag{37}$$

$$U = K \sin^2\Psi \sin 2\phi \tag{39}$$

To find the mean values, $\bar{I}$, $\bar{Q}$ and $\bar{U}$ over the whole ring, we integrate with α going from 0 to 2π, noting from figure 2.6(a) that the angles Ψ and ϕ can be expressed in terms of α and i by

$$\cos\Psi = \cos\alpha \,.\, \sin i \tag{40}$$

$$\sin\alpha = \cos\phi \,.\, \sin\Psi \tag{41}$$

so that

$$\bar{I} = \frac{K}{2\pi}\int_0^{2\pi} (1 + \cos^2\alpha \,.\, \sin^2 i)\, d\alpha = \frac{K}{2}(2 + \sin^2 i) \tag{42}$$

$$\bar{Q} = \frac{K}{2\pi}\int_0^{2\pi} (\sin^2\alpha - \cos^2\alpha \,.\, \cos^2 i)\, d\alpha = \frac{K}{2}\sin^2 i \tag{43}$$

$$\bar{U} = \frac{K}{2\pi}\int_0^{2\pi} \sin 2\alpha \,.\, \cos i \,.\, d\alpha = 0 \tag{44}$$

Therefore, the mean polarization, $\bar{p}$, is then

$$\bar{p} = \frac{\sqrt{\bar{Q}^2 + \bar{U}^2}}{\bar{I}} = \frac{\sin^2 i}{(2 + \sin^2 i)} \tag{45}$$

and is <u>normal</u> to the orbital plane as signified by $\bar{U}$ being zero and $\bar{Q}$ being positive, (see section 2.2.1.). Therefore, measurement of the polarization angle gives directly the orbital position angle with respect to north.

For the case of an eclipsing binary, where i is close to 90°, $\bar{p}$ will be close to $\frac{1}{3}$. So far only a single thin ring has been considered. The

polarization over the whole disk is obtained by summing the contributions from the series of concentric rings. As only a geometrical scaling factor changes when going from one ring to the next, each ring will have the same net polarization and the overall disk polarization is

$$p_{disk} = \frac{\sin^2 i}{(2+\sin^2 i)} \qquad (46)$$

However, it is unlikely that the disk remains optically thin everywhere, with the result that secondary scattering must be allowed for. This reduces the maximum p_{disk} to below $\frac{1}{3}$. There is considerable doubt on how much this reduction should be, although Piirola (1975) suggested that a realistic maximum for p_{disk} is 1/10.

The above analysis is idealized in that radiation from the secondary star has been omitted and the circumstellar envelope has been assumed strongly concentrated towards the orbital plane. These limitations are not thought to be too important for systems such as U Cephei and Beta Lyrae, in which the scattering material forms an accretion disk around one of the stars.

If the inclination of the orbit is zero, there will be no net polarization from this mechanism. In this case, polarization can only be produced by the reflection effect, in which radiation from the brighter star is scattered and reradiated by the fainter companion. The interesting feature here is that the amount of polarization remains constant with orbital phase, but the plane of polarization rotates twice through 180° during

one complete orbital period. This is perhaps the only way of detecting a pole-on binary system.

Apart from the two limitations mentioned above, there is a third weakness in this circumstellar model. In general the scattering material will not be distributed uniformly around either star, but will tend to be much denser in the vicinity of the inner Lagrangian point. A more realistic model based on a non-uniform envelope has recently been developed by the group at the University of Oregon and will be considered next.

2.2.3 Scattering in a non-uniform circumstellar envelope

Rudy and Kemp (1976, 1978) have constructed a model to predict the polarization from a non-uniform circumstellar envelope composed of discrete scatterers. Their model includes the effect of both stars in a binary system and is not restricted to scattering in the orbital plane.

The details of their model are to be found in Appendix A, but the essential points are as follows. As mentioned in the previous section, a binary inclined at 90° (i.e., edge on) will have a maximum integrated polarization of $\frac{1}{3}$, with the electric vector perpendicular to the orbital plane. If a single scattering electron were traced around the complete orbital path, the polarization of its scattered flux would vary smoothly from zero at phases 0.0 and 0.50 to a maximum at quadrature (phases 0.25 and 0.75). This is represented by a straight line in the Q, U plane as shown in figure

2.7(a). For a pole-on system (figure 2.7(b)) the magnitude of the polarization would remain constant over the orbital period, but the orientation of the plane of polarization would change continually. This is indicated by a circle in the Q,U plane. An intermediate inclination would give an ellipse as shown in figure 2.7(c). The orientation of the ellipse gives directly the position angle of the orbital plane.

To be exact, for the case of a single scatterer illuminated by one star, the ellipse has the form

$$\left[\frac{Q - (A_1/\Phi_o)\,\frac{\sin^2 i}{2}}{(1 + \cos^2 i)/2}\right]^2 + \frac{U^2}{\cos^2 i} = \frac{A_1^2}{\Phi_o} \qquad (47)$$

where Q, U, Φ_o and i have the same meaning as before. The quantity A_1 is the product of two constants, one equal to the fraction of total light scattered, and the other taking into account the finite size of the central star. This ellipse is actually two coincident ellipses, since points separated by 0.5 phase are degenerate, i.e. have identical Stokes parameters. The eccentricity of the ellipse is equal to $(\sin^2 i/(\cos^2 i + 1))^{\frac{1}{2}}$, so that the orbital inclination can also be obtained from the Q,U plot.

Extending the model to multiple scatterers and adding the contributions from both stars gives the elliptical form

$$\left[\frac{Q - (m\bar{A}/\Phi_o)\,\sin^2 i}{(1 + \cos^2 i)/2}\right]^2 + \frac{U^2}{\cos^2 i} = \frac{S_1^2 + S_2^2}{\Phi_o^2} \qquad (48)$$

where $\bar{A}$ is the mean value of $A_{1,2}$ over m individual scatterers, and $S_{1,2}$ are geometrical factors describing the distribution of scatterers around the two stars.

This gives the important result that the extension from a single scatterer to a finite scattering region does not distort the elliptical plot in the Q,U plane; only the relative size is changed.

Furthermore, for a symmetric ring of particles, where $S_1 = S_2 = 0$, the ellipse collapses to a single point,

$$U = 0, \quad Q = (m\bar{A}/\Phi_o) \sin^2 i, \qquad (49)$$

identical to the result found in the previous section for the case of the uniform circumstellar disk.

A typical Q,U plot is shown in figure 2.8 for the system, AO Cassiopeiae, and taken from Rudy and Kemp (1978). The conjunction points (phases 0.0 and 0.5) are essentially degenerate, which means that the scattering matter must be near to the orbital plane. The quadrature points (phases 0.25 and 0.75) are significantly different and suggest that the densest part of the circumstellar disk is not at the inner Lagrangian point, but nearer the trailing or advancing edge of the secondary star, such that at phase 0.25, this part of the disk is partially eclipsed by the secondary. Finally the difference in polarization between phases 0.25 and 0.75 enabled Rudy and Kemp to estimate the scattering mass as 3×10^{-10} solar masses.

2.3 Other sources of polarization

There are several other astronomical sources of polarization having their origin in either magnetic or general relativistic effects.

2.3.1 Magnetic effects

The Zeeman effect, in which a spectral line is split into several equally spaced lines, the centre line linearly polarized in the direction of the magnetic field, the other lines circularly polarized in opposite directions, has been observed in recent years.

The transverse Zeeman effect, in which the circularly polarized satellite lines are seen as linearly polarized lines orthogonal to the centre line, has been observed in magnetic Ap stars by Kemp and Wolstencroft (1973). The effect was observed in the H_β line, in which the central part of the line was saturated, thus giving a net polarization due to the wings.

In highly magnetized stars, the circularly polarized Zeeman components are sufficiently separated that they can be resolved. This so-called transverse Zeeman effect has been observed in many white dwarfs (Landstreet, 1974).

2.3.2 General Relativistic effects

The Einstein photometric effect, or 'gravitational focussing' as it is

sometimes called, of a black hole orbiting around a bright central star is equivalent to a scan across the surface of the bright star. Dolan (1976) has pointed out that this would allow the limb polarization, predicted by Chandrasekhar (1946), to be seen directly. This effect has been looked for in Cygnus X-1 by Dolan, but not seen. In fact, the perfect alignment of bright star, black hole and observer required, make it very unlikely that the effect will ever be seen.

All electromagnetic radiation can be represented as the sum of left and right handed circularly polarized components. A rotating black hole will absorb that handedness of radiation which slows its rotation down more easily than that which speeds it up so that radiation scattered by a rotating black hole should be circularly polarized to some extent. This effect has also not yet been seen.

In conclusion, all linear polarimetric observations made so far have been successfully explained by one of the above models. In particular, the discussion of the present work, which takes place in Chapter 5, will refer to the models of Davis and Greenstein (1951), Shakhovskoi (1965) and Rudy and Kemp (1978).

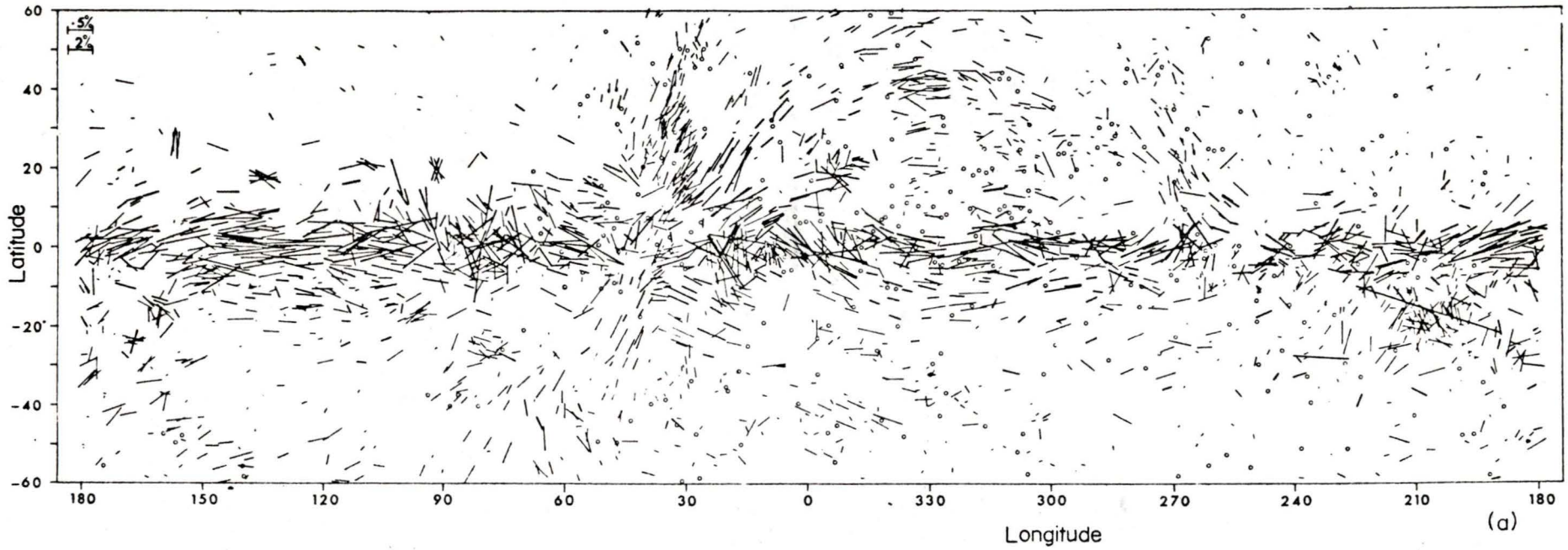

Fig. 2.1 Interstellar polarization in galactic coordinates. The stars measured are at the centre of each line. The length of each line is proportional to the percentage polarization and the orientation of the line represents the direction of the electric vector.
(Reproduced with permission from Memoirs R.A.S., 74, 143.)

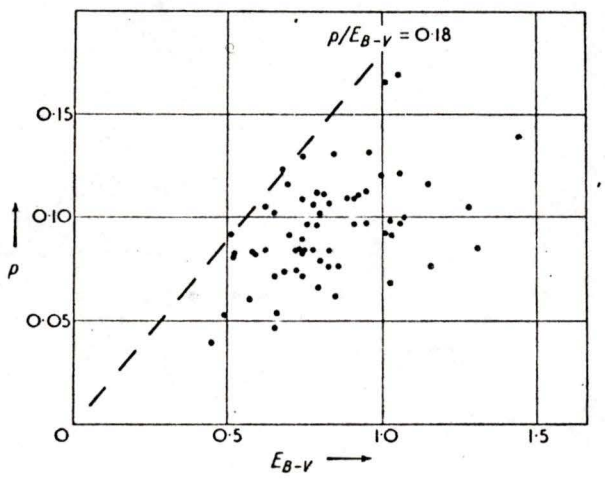

Fig. 2.2 Polarization versus colour excess for the Cassiopeia region. A line with a slope equal to 0.18 has been drawn to correspond to an acceptable observed maximum for the ratio of polarization to colour excess. (Reproduced with permission from Vistas in Astronomy, 2, 1089.)

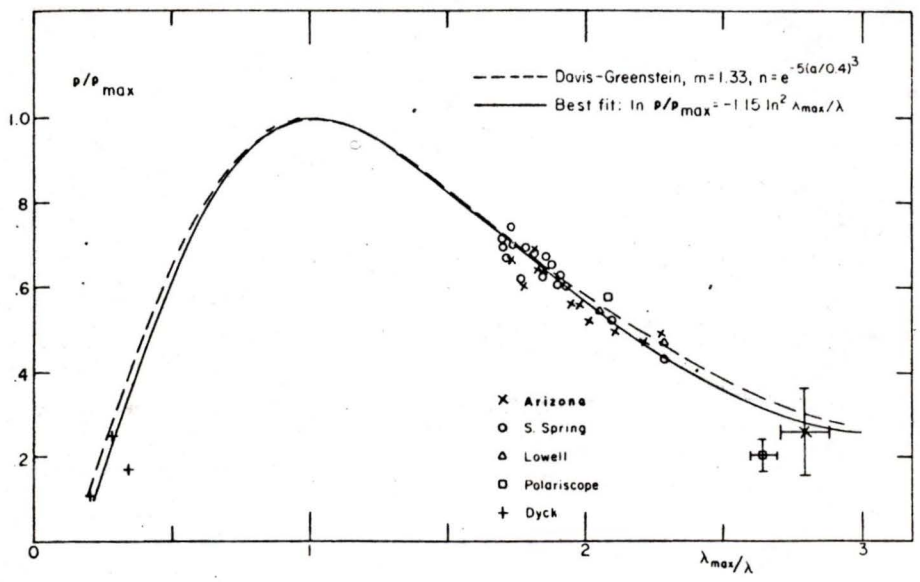

Fig. 2.3 The wavelength dependence of interstellar polarization. (Reproduced with permission from 'Planets, Stars and Nebulae, ...' ed. T. Gehrels, University of Arizona Press, p. 895.)

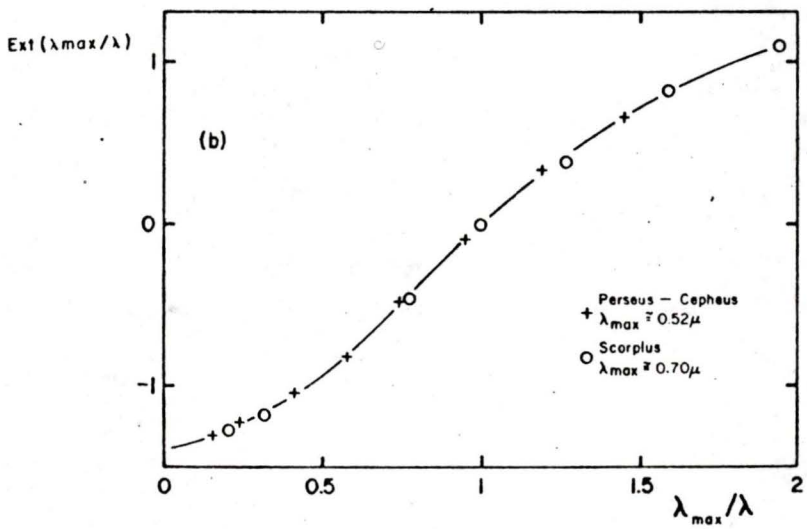

Fig. 2.4 The wavelength dependence of interstellar extinction. (Reproduced with permission from 'Planets, Stars and Nebulae, ...' ed. T. Gehrels, University of Arizona Press, p. 888.)

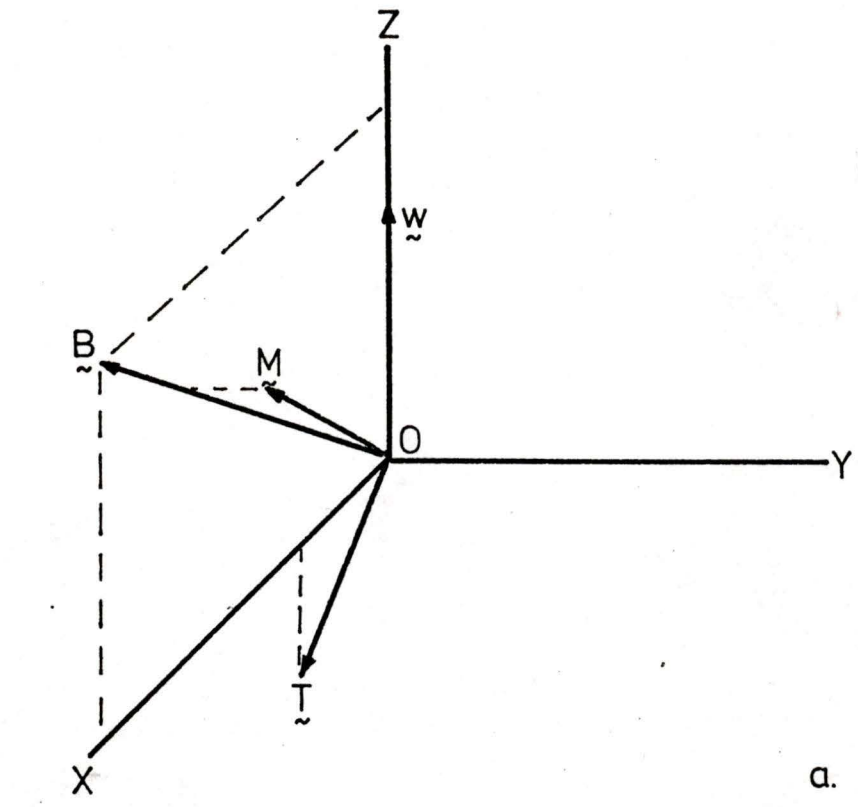

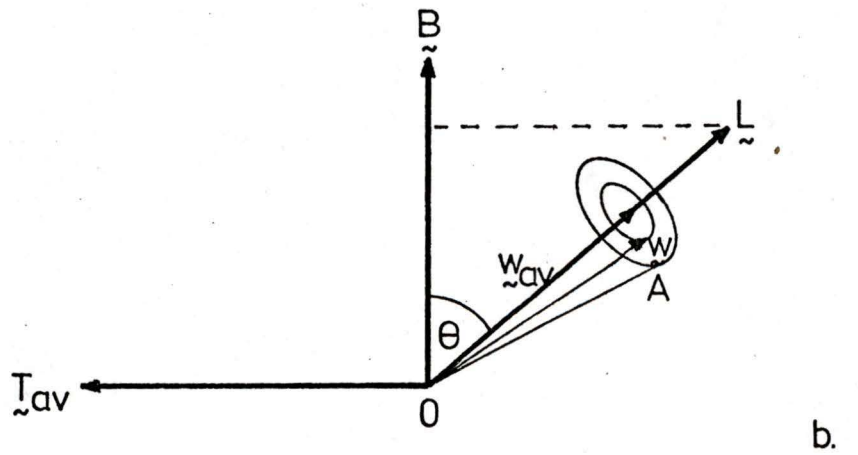

Fig. 2.5. Magnetic alignment geometry

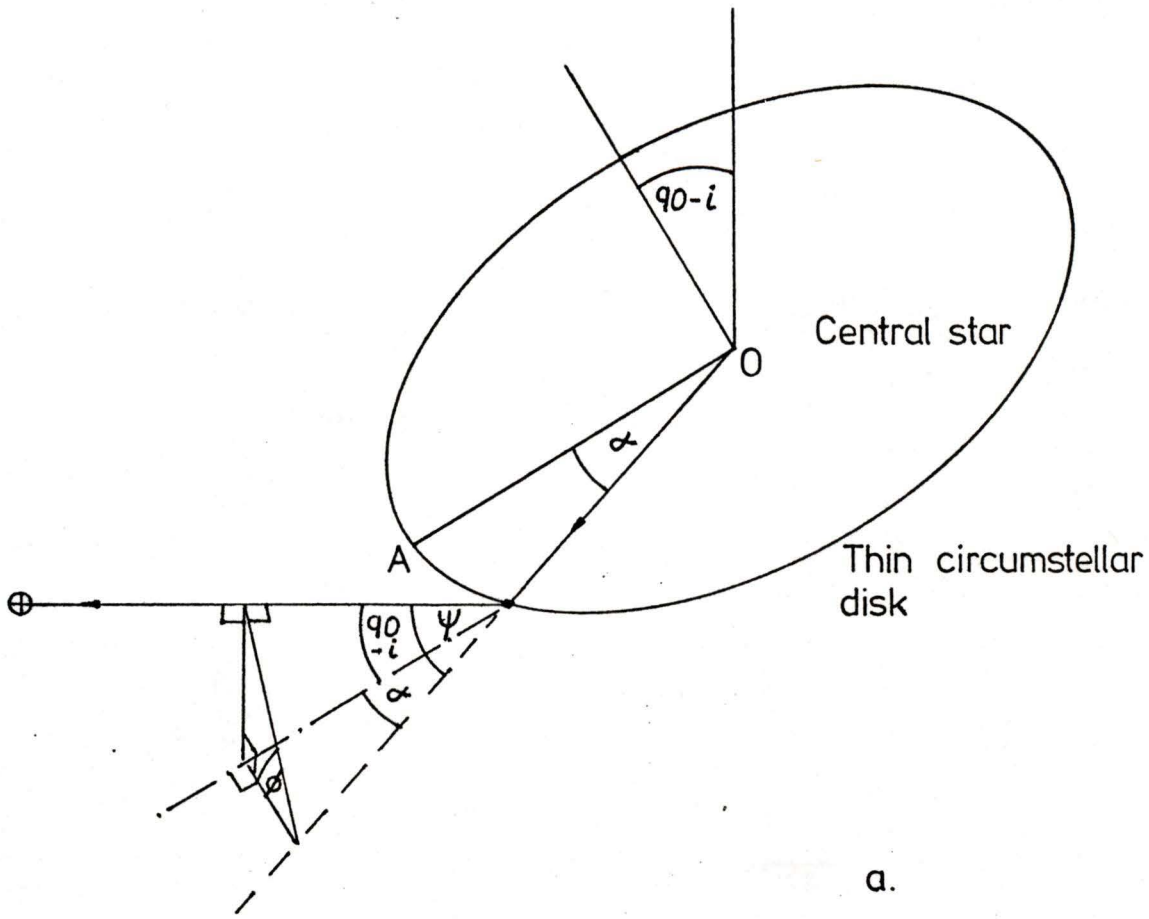

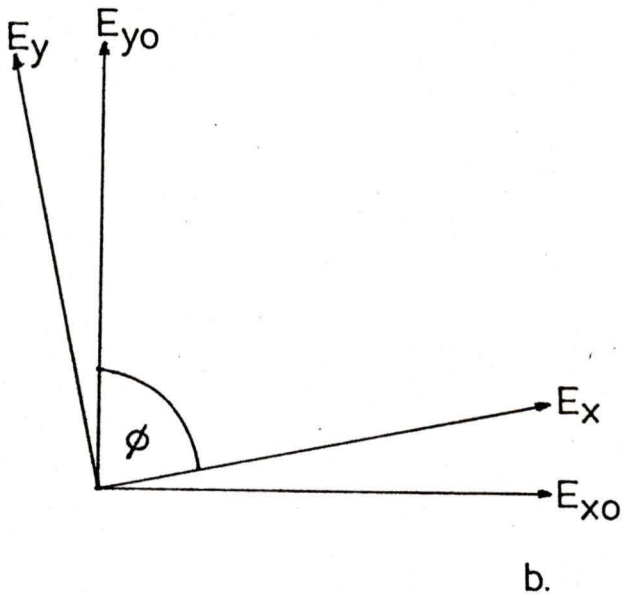

Fig. 2.6. Scattering geometry of a thin disk

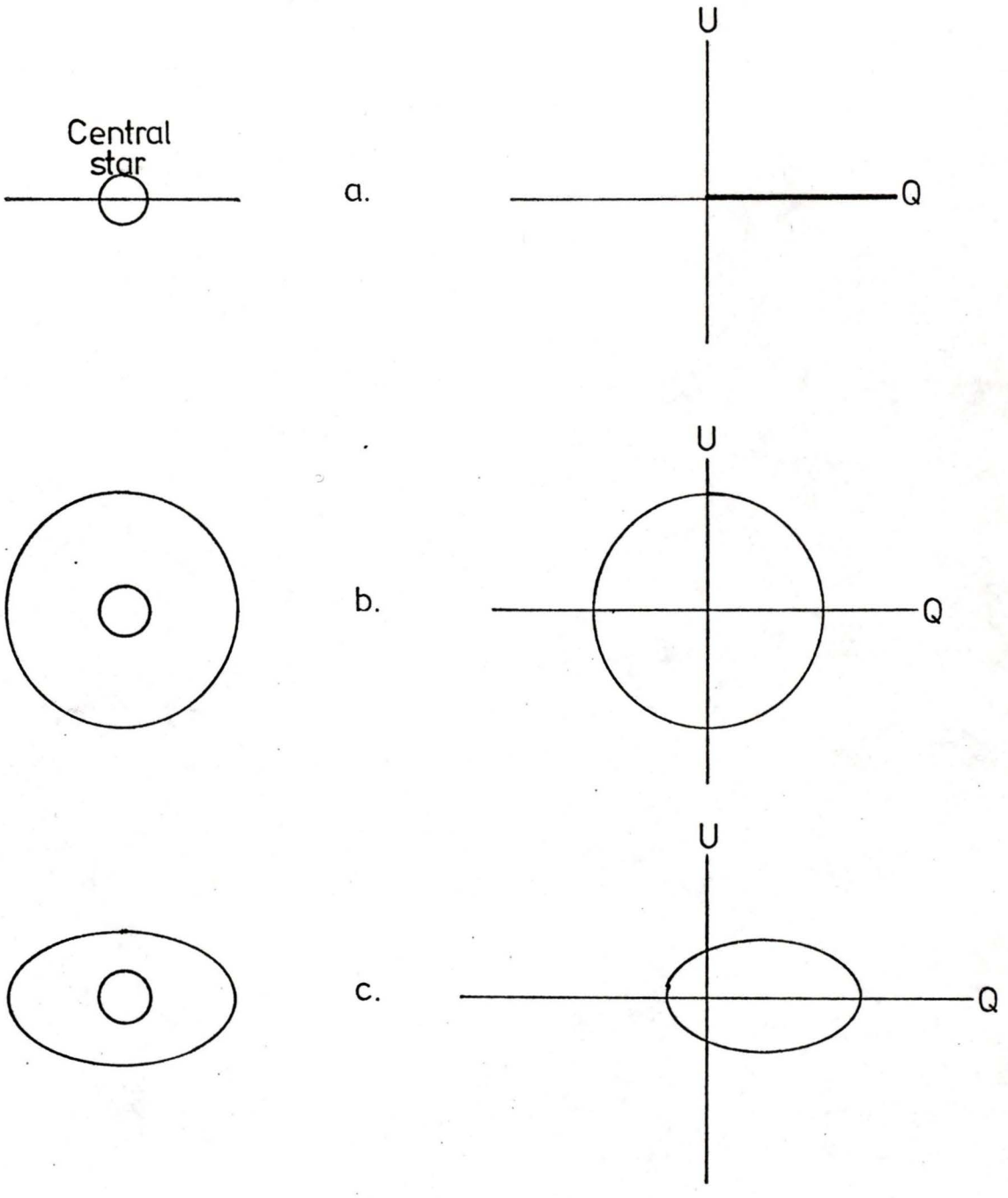

Fig. 2.7. Theoretical Q , U plots

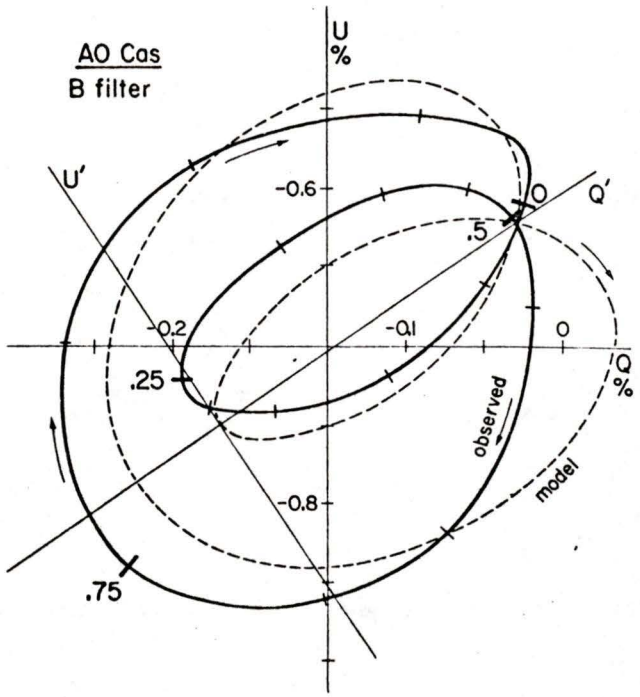

Fig. 2.8 The Q,U plot for AO Cassiopeiae. Tick marks show phase intervals of 0.05. The dashed path is computed from the scattering model. The solid path represents the smoothed observations.
(Reproduced with permission from Ap. J., 207, L126.)

CHAPTER 3 EXPERIMENTAL POLARIMETRY

Ideally, it should be possible to measure the linear polarization of a star by rotating a polaroid in front of the star until the star appears brightest and measuring this brightness, and then rotating the polaroid through 90^{o} and again measuring the stellar brightness. The degree of polarization is then the difference in brightness over the sum of the brightness, with the position of the polaroid for maximum brightness defining the plane of polarization. All polarimeters work on this general principle but several sources of error tend to complicate the design of practical instruments.

3.1 Sources of error in polarimetry

This section is based on an excellent review of the errors in modern polarimetry by Serkowski (1974).

3.1.1 Atmospheric scintillation and seeing

Since air is not birefringent, scintillation is the same for both orthogonally polarized componenents of light from an astronomical object. The ratio of intensities of the two components is free of the effects of atmospheric scintillation and is not affected by the presence of thin clouds. The accuracy of polarimetry through clouds is reduced only because of fluctuations in sky background and the smaller number of photons received.

Atmospheric seeing is a more serious problem, largely because of image

motion on the polarimetric analyzer (e.g. polaroid) and the following photo-detector. If the optics are such that an image of the primary telescope mirror is formed on the detector, the rapidly changing distribution of illumination of this image (usually called the shadow pattern) causes fluctuations in the output of a spatially nonuniform detector.

One remedy is to split the polarized light into orthogonal beams by means of a Wollaston prism and then take the instantaneous ratio of the two beams. The Wollaston prism is constructed of two individual prisms cemented together with their optic axes perpendicular (see figure 3.1) and having the property that the orthogonal components of the incoming beam of light are split into two separate beams. By employing two identical detectors to take the ratio, most of the atmospheric modulation can be eliminated.

A better remedy is to rapidly rotate, either mechanically or electronically, the analyzer such that the stellar image is effectively 'frozen' while the orthogonal intensity readings are being taken. This approach has the great advantages that only one detector is required and that the polarization information is modulated, making detection in the presence of noise so much easier. This is the principle underlying the present polarimeter.

3.1.2 Image motion on the detector

Apart from that caused by atmospheric seeing, image motion can also be

caused by the rotation of any optical element which is not plane parallel to the detector. The best solution is to electronically rotate an optical element such as a Pockels cell. Another approach is to use a rotating optical element which modulates any polarimetric information at a multiple of the mechanical rotation rate, and then follow with a signal processing scheme sensitive only to the modulation frequency. Most photocathodes are somewhat sensitive to the state of polarization of the incoming light, so that the rotating analyzer must be followed by a depolarizer.

3.1.3 Instrument polarization

Linear polarization from the mirrors of a Cassegrain telescope usually does not exceed 0.1%, provided the mirrors have been uniformly aluminized. A potentially more serious problem is the conversion of linear to circular polarization by the telescope optics. Such linear-to-circular conversion diminishes the measured degree of linear polarization for the object observed, rotates the plane of polarization and causes instrumental circular polarization.

The ideal optical arrangement is to have neither lenses, filters nor tilted mirrors before the polarimetric analyzer. It is for this reason that Newtonian telescopes are rarely used, although theoretically the linear polarization and linear-to-circular conversion produced by the tilted flat mirror could be allowed for.

3.1.4 Photon noise

Provided the instrumental polarization is small ($< 0.2\%$), the principal limitation to polarimetric precision comes from photon statistics. For example, to measure the linear polarization of an object to 0.1% requires the photon statistical uncertainty to be better than 0.01%, or the total number of photons collected to be greater than 10^8. For this reason, the higher quantum efficiency detectors such as silicon vidicon television cameras and semiconductor diode arrays are coming into use. Splitting up the spectrum to do spectropolarimetry makes the problem even worse, and only bright stars ($V < 8$) have been routinely observed so far.

3.2 Types of polarimeters

The earliest polarimeters were simple devices. Hiltner (1956a) used a Glan-Thompson prism (which passes only one direction of linearly polarized light) rotated in discrete steps, followed by a depolarizer and photomultiplier tube. At each discrete step of the prism, the signal was averaged to reduce the effects of scintillation and seeing. Even so, this system was capable of measuring only large ($> 1\%$) degrees of linear polarization.

Hall (1949) also used a Glan-Thompson prism analyzer, but rotated it continuously at 15 Hz. Any linear polarization showed up as a 30 Hz sine wave trace on a pen recorder, which was connected via an amplifier to the output of the photomultiplier tube.

Angel and Landstreet (1970) have made many observations using a Pockels cell as an electronically rotatable waveplate, followed by a Wollaston prism analyzer. The Pockels cell consists of a transparent crystal of potassium dihydrogen phosphate, across which a longitudinal potential difference is applied. The birefringence (difference in refractive index for orthogonal polarizations) of the crystal is directly proportional to the applied voltage, and thus the crystal can act as either a quarter wave plate (in which the two orthogonally polarized rays suffer a relative phase shift of 90°) or a half wave plate (in which the relative

phase shift is 180°). A relative phase shift of 90° causes a transformation from circular to linear polarization, and vice versa, whereas a 180° shift rotates the plane of polarization through 90°. The voltage applied to the Pockels cell is pulsed so that any polarization shows as a modulation of the output from the Wollaston prism.

Figure 3.2 shows the optical layout of a dual channel polarimeter built by Clarke and McLean (1975). The Double Beam Polarizer splits the incoming beam into its orthogonal components in a way similar to that of the Wollaston prism. The instantaneous difference in output of the two photomultiplier tubes is proportional to the degree of linear polarization and is said to be virtually unaffected by atmospheric effects. A movable half wave plate rotates the plane of polarization applied to the D. B. Polarizer to eliminate systematic instrumental polarization. Circular polarization is measured by inserting a quarter wave plate into the light path. Tiltable filters are used for narrow band spectropolarimetry.

Finally, figure 3.3 shows a schematic drawing of possibly the most accurate and versatile type of polarimeter so far constructed (Stokes et al., 1976). The heart of the instrument is a photoelastic modulator invented by Kemp (1969), followed by a Glan-Thompson analyzer. The photoelastic modulator consists of a piezoelectric crystal cemented to a bar of fused silica such that when the crystal vibrates at its natural frequency (close to 50 kHz), the birefringence of the silica also changes simulating both

quarter and half wave plates rotating at different harmonics of the basic 50 kHz frequency. This rapid multi-harmonic modulation permits simultaneous measurement of linear and circular polarization completely free of atmospheric effects.

3.3 The present polarimeter

The constituent parts of the instrument used in the present work will now be considered.

3.3.1 The optics

The polarimeter head which includes the optics, photodiode detector and head amplifier is shown in figure 3.4. Light from the 31 cm Cassegrain telescope of the University of Victoria Observatory is reflected from the telescope secondary mirror through the entrance aperture of the polarimeter and comes to a focus at the focal plane diaphragm. This is a multi-position rotary wheel containing five apertures of diameters 0, 33, 65, 130 and 260 arc seconds. A sixth position contains a piece of polaroid of known orientation for use in checking the operation of the system. The focal plane image can be viewed with the aid of a flip mirror, imaging lens and eyepiece. Diverging light from the focal plane passes through the rotating polaroid, the field lens, the bandpass filters (if used) and onto the active area of the photodiode detector. Immediately behind the detector is mounted a low noise amplifier. Signals from the amplifier pass via a cable down to the main signal processing unit.

The polaroid is a circular piece of HN-32, manufactured by the Polaroid Corporation. The transmittance of light linearly polarized parallel to the maximum transmission axis of the polaroid is fairly constant at 72 $\pm$ 5%

over the 500 to 700 nm. region of the spectrum. The transmittance of the orthogonal polarization is less than 0.005% over the same wavelength range but rises steeply at either end of the range. In fact, longwards of 800nm. the polaroid is quite ineffective as an analyzer. For this reason, an infra-red absorbing filter is inserted into the light path to remove all wavelengths longer than 750 nm. Preceding the infra-red filter, there is a field lens to focus the light onto the sensitive area of the detector, and following the i.r. filter, there is a filter wheel containing Schott glass filters to give the standard Johnson U, B, V, R, I spectral band-pass sequence. The sixth position on the filter wheel is open and, because of the limited aperture of the 31 cm. telescope, this was the normal mode of operation.

The photodiode detector is a low noise PIN silicon diode manufactured by United Detector Technology Inc. of Santa Monica, California. The low noise is achieved by having an active area of only 2×10^{-7} m^2; however, this small size does magnify the tracking problems present with any telescope. In particular, for the 31 cm. telescope it was found difficult to keep the stellar image centred on the diode for much more than a few minutes, and this alone was responsible for limiting the maximum integration time to 30 seconds. The detector was found to be insensitive to the state of polarization down to below the 0.1% level and so no depolarizer was used. Figure 3.5 shows the combined spectral response of the i.r. filter and the detector, the passband ripple being due to the

interference filter. The half height spectral range is 478 to 724 nm.

Figure 3.6 shows the polarimeter head mounted on the 31 cm. telescope, together with the signal processor. To estimate the scale of the photograph, the tube connecting the head to the telescope is 6 cm. in diameter.

3.3.2 The electronics

The output of the polarimeter head comprises three signals, a d.c. voltage proportional to the average light intensity, an a.c. voltage proportional to the degree of linear polarization and a random noise component due to the imperfect nature of both the detector/amplifier and the atmosphere. The electronic signal processor has the task of determing the average light intensity, the degree of linear polarization and the orientation of the plane of polarization, all in the presence of noise which is often several times greater than the polarimetric signal.

The detailed circuit diagram appears in Appendix B and a functional block diagram in figure 3.7. Referring to this figure, the frequency of the electric motor (and hence the rotating polaroid) is kept within one hertz of 68 Hz by a feedback controller. This 68 Hz signal is also used as a master synchronizing signal by the digital part of the circuitry. The rotating polaroid converts any linear polarization into a 136 Hz alternating current in the photodiode. The head amplifier converts this current

to a voltage while transferring the signal impedance to a low value for transmission to the main signal processor. There the sky background is removed and the signal amplified. The a.c. and d.c. components of the signal are separated by means of active filters. The atmosphere noise shows up as a random modulation with a frequency spectrum extending from zero to about 40 Hz. The active filters pass this modulation without seriously changing the relative phase of the various frequency components, so that when the a.c. and d.c. signals are subsequently electronically divided, the atmospheric noise is essentially cancelled.

The polarization signal has still to be recovered, often from under the noise contributed by the photodiode and head amplifier. However, the frequency of the polarization signal is known to be 136 Hz, and so can be recovered in a synchronous detector sensitive only to this frequency. As this detector is driven by a signal from the electric motor, any variation in motor speed due to environmental or positional changes is reflected by a corresponding change in the centre frequency of the synchronous detector. The detector output is filtered, integrated and finally displayed as the degree of polarization.

The difference in zero crossing time between the synchronous detector output and motor reference signal, expressed in degrees between zero and 179.9°, gives the orientation of the plane of polarization. The phase of the motor reference signal can be arbitrarily shifted for calibration purposes.

3.3.3 Instrumental specifications

The total instrumental polarization was measured in the laboratory as being less than 0.2%, the difficulty at these small levels being to distinguish between the residual polarization of the light source and that of the polarimeter. The polarization angle can be measured to $\pm$ 0.1°, as determined from observations of the daylight sky polarization. The overall sensitivity of the system is set by the aperture of the telescope and the noise in the detector/head amplifier. The total system noise corresponds to 0.2% polarization of a 5th magnitude class B star. Cooling the detector would have reduced the noise by one to two orders of magnitude, but was not possible due to physical limitations.

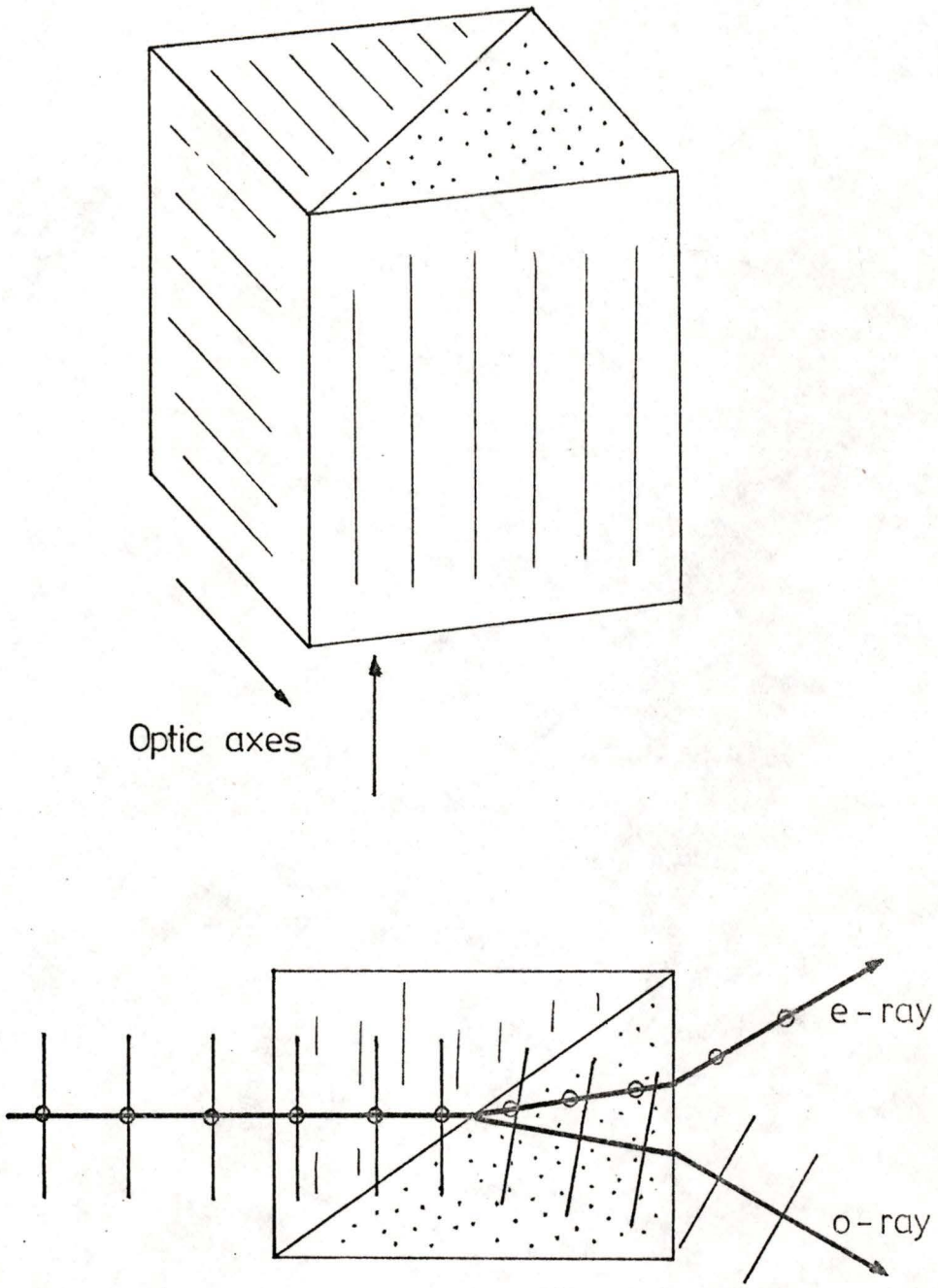

Fig. 3.1. The Wollaston prism

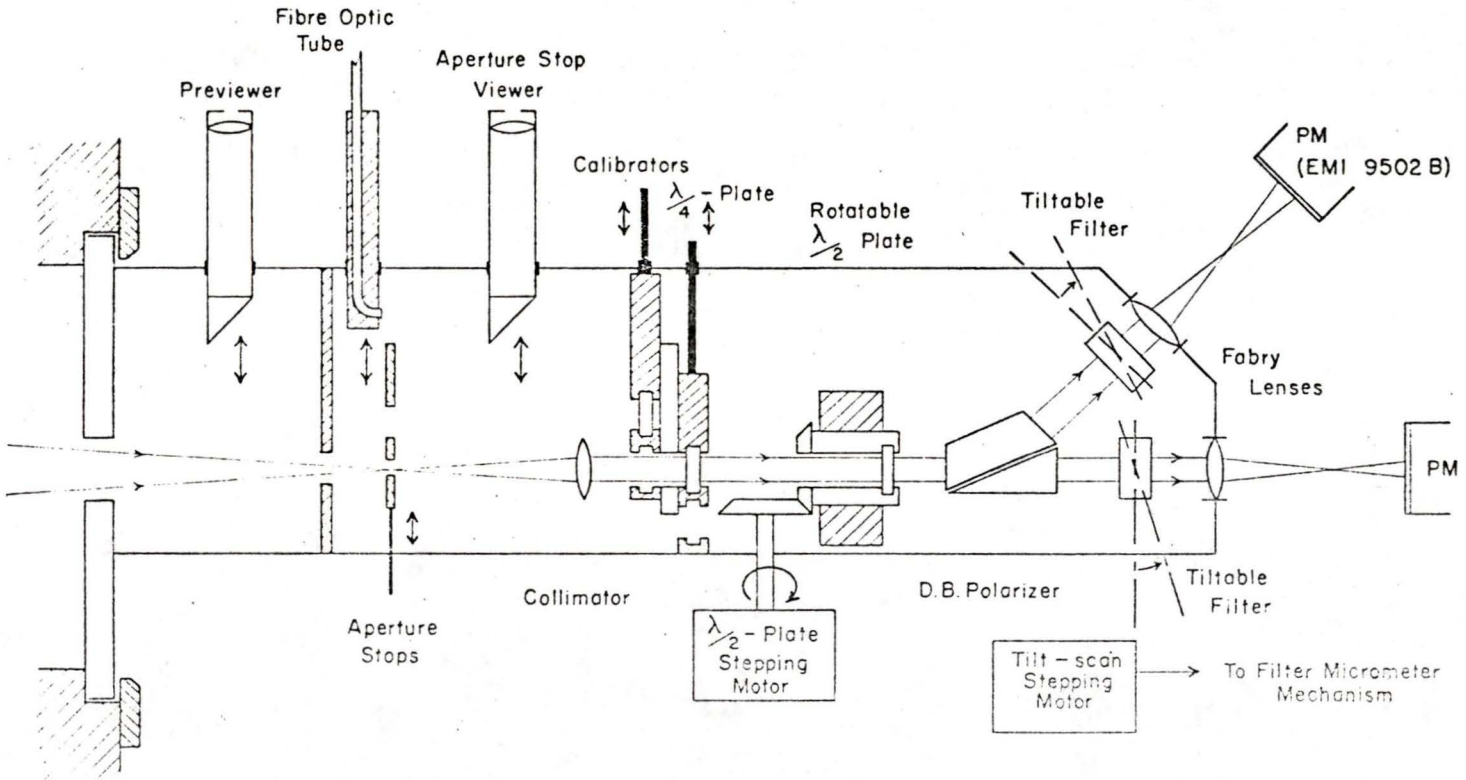

Fig. 3.2 The optical layout of the dual marrow-band wavelength scanning polarimeter. (Reproduced with permission from M.N.R.A.S., 172, 547.)

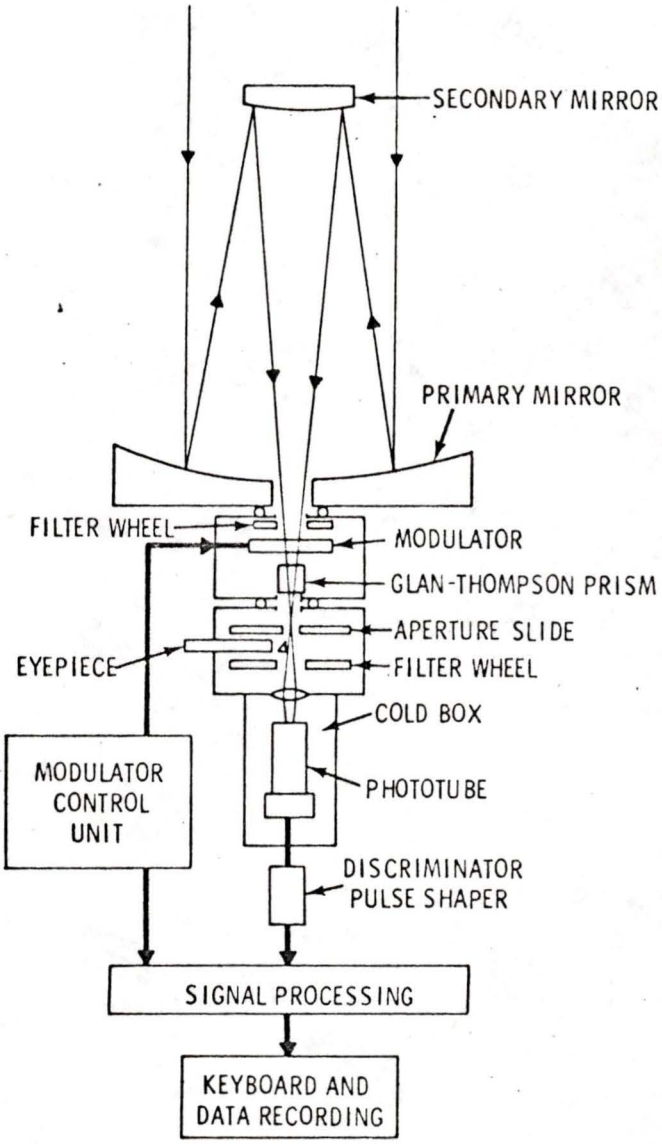

Fig. 3.3 The polarimeter of Stokes, Ekstrom and Swedland. (Reproduced with permission from Optical Engineering, 15, 8.)

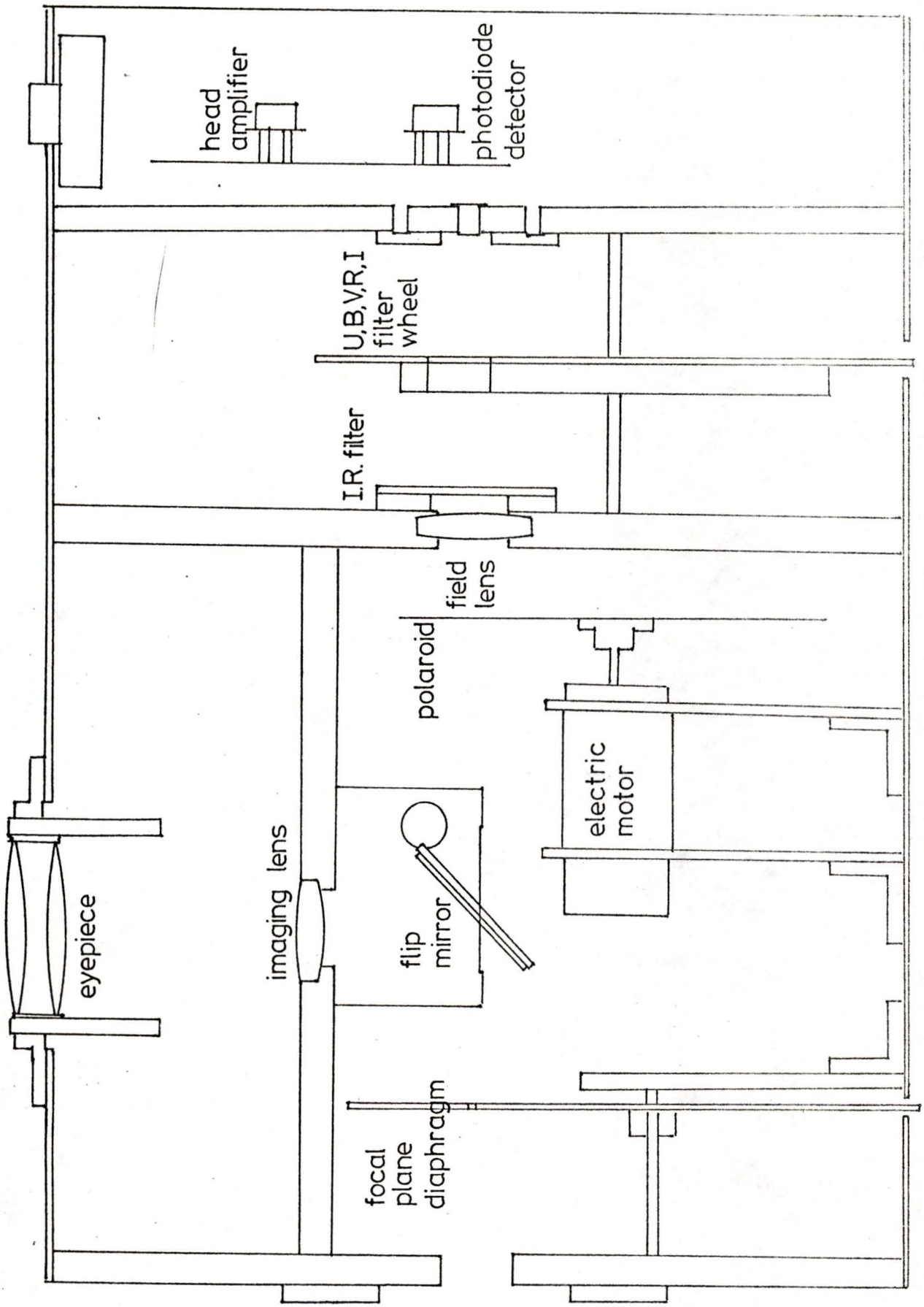

Fig. 3.4. Physical layout of present polarimeter head (Full size)

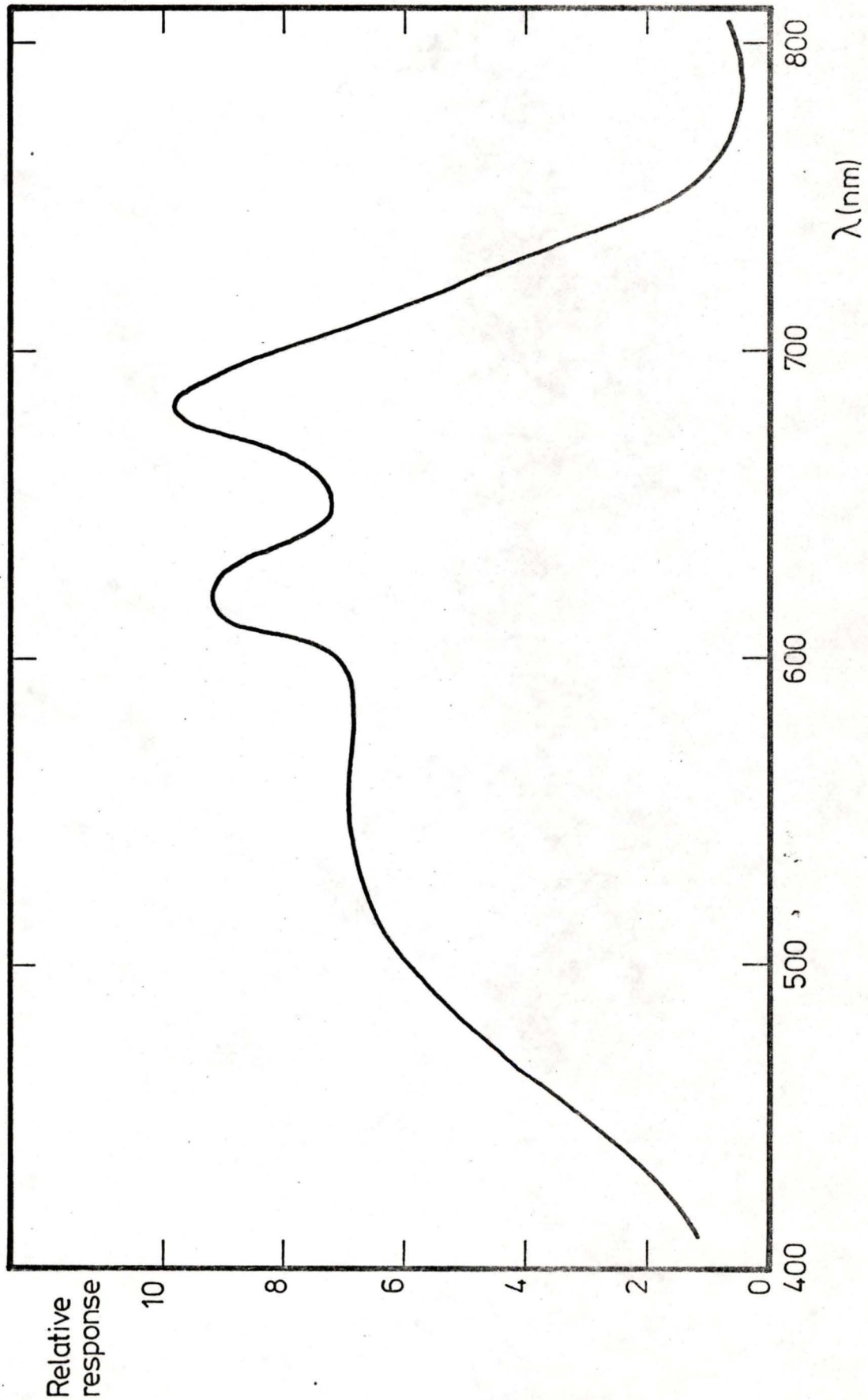

Fig. 3.5. Spectral response of photodiode / I.R. filter

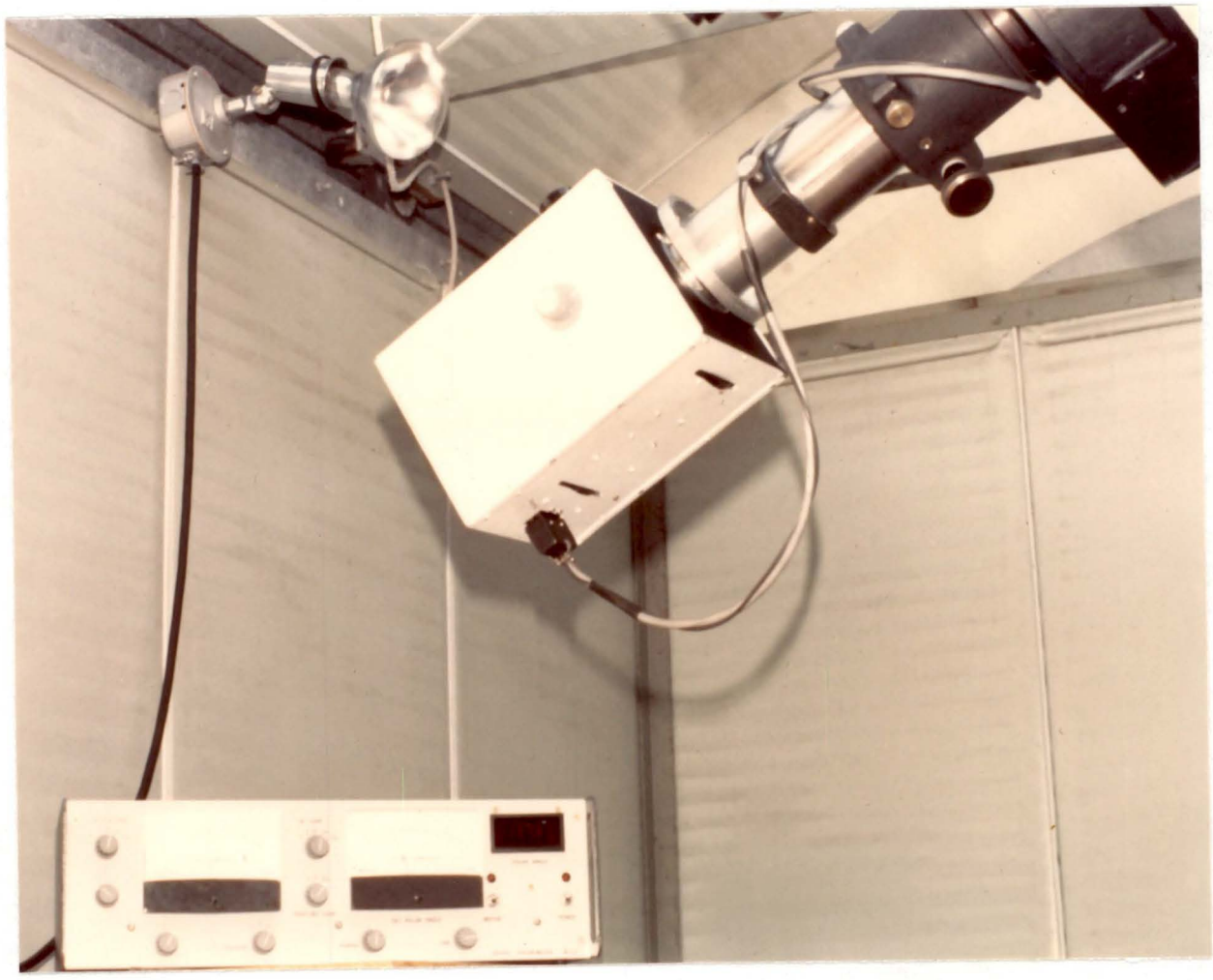

Fig. 3.6 Photograph of the present polarimeter. The instrument is mounted on the 31 cm telescope of the University of Victoria Observatory.

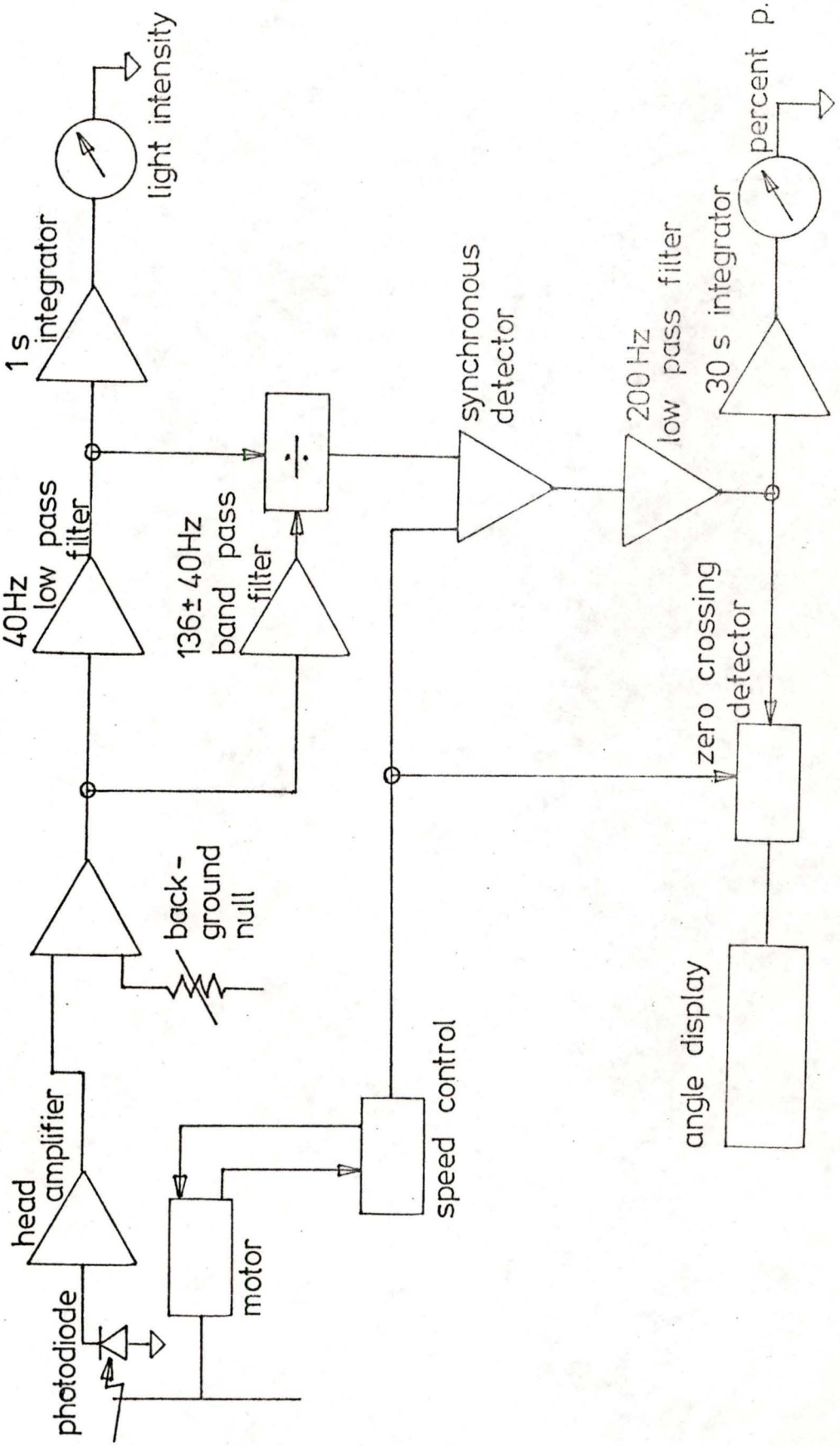

Fig. 3.7. Block diagram of electronics of present polarimeter

CHAPTER 4 OBSERVATIONAL RESULTS

Before commencing the observing programme, it was necessary to calibrate the polarimeter. This was accomplished by observing several standard stars whose linear polarization had been measured by previous observers (Serkowski, 1974; Treanor, 1963; Coyne et al., 1974) and are considered well established.

4.1 Calibration stars

Five polarized and three non-polarized stars were measured prior to the observations, and checked repeatedly during the course of the observations. The measured polarizations of the eight standard stars together with their established ('true') polarizations are shown in table I.

Two points are immediately obvious; the minimum or residual polarization of the system is approximately 0.18%, and the measured value of polarization is always lower than the 'true' value. The residual polarization of 0.18% has a large randomness in it. In particular, for the case of Alpha Lyrae, the residual polarization was measured on nine separate nights and ranged from a low of 0.04% to a high of 0.40%. There was some correlation between the polarization and the state of the atmosphere, in that the lowest values occurred on nights with the lowest scintillation and best seeing. Furthermore, the polarization angle was variable, suggesting that not just

instrumental polarization was being measured. The most likely explanation of this residual lies in a combination of three separate effects:

(i) incomplete cancellation of the atmospheric modulation,

(ii) image motion on the detector due to the rotating polaroid,

(iii) instrumental polarization of about 0.04%.

The result is that the minimum detectable polarization is about 0.2%. It is interesting to note that the polarization of Deneb was measured to be 0.36% or, removing the instrumental contribution, a net value of 0.31%. The measured position angle of 2^{o} is very close to the position angle of 3^{o} quoted for the nearby star, 55 Cygni, and confirms the ability of the polarimeter to measure small levels of linear polarization.

Table I also lists the spectral class and colour of the five standard polarized stars, and it can be seen that there is a correlation between the ratio of 'true' to measured polarization and both spectral class and colour. This is seen better in figures 4.1 and 4.2. The correlation with spectral class is very high and suggests the following explanation. In chapter 3 it was mentioned that the polaroid is not very efficient at long wavelengths. This inefficiency shows up as an artificial lowering of the measured polarization. Now, the later the spectral class, the greater the fraction of energy falling in the red part of the spectrum, and the lower will appear the measured polarization. The same argument applies to the colour plot, figure 4.2. For all five stars the source of polarization is interstellar with the maximum

occurring within the narrow wavelength interval of 510 to 560 nm., so the effect cannot be due to the spectral shape of interstellar polarization. It should be noted that this effect is an artifact of the imperfect nature of the polaroid and is not seen in polarimeters employing achromatic modulators/analyzers.

The polarization angle was calibrated by observing the zenith sky polarization at sunset at which time the sky is linearly polarized in a direction normal to the direction of the sun. The measured angles shown in table 4.1 are sufficiently close to the 'true' values that no corrections have been applied.

4.2 The supergiant stars

The three supergiant stars, 89 Herculis, Rho Cassiopeiae and HD 217476, were observed over the period July to December, 1977 and, in the case of 89 Her, again in May, 1978.

On no occasion was any net polarization measured for 89 Her, which means in practice that the polarization must have been less than 0.2%. This was also the case for the nearby stars, 83 Her, 84 Her, and 87 Her suggesting that either the interstellar magnetic field is weak in this region of the galaxy, or there is very little interstellar dust or the field lines are 'jumbled'.

Linear polarization was observed for both ρCas and HD 217476. Instrumental calibration factors of 1.56, for ρCas, and 1.63, for HD 217476, were taken from figure 4.1. The corrected observations of both percentage polarization and position angle, θ, are listed in table II and plotted in figures 4.3 and 4.4. In both cases, there is no significant deviation from mean values of, in the case of ρCas, 1.44% and 53°, and in the case of HD 217476, 3.18% and 64°. These results are discussed further in the next chapter.

4.3 Beta Lyrae

This well known binary was observed on 12 nights. The observations are listed in table III. Owing to the impossibility of assigning a constant spectral class throughout the orbital cycle, no correction factor has been applied. In any case the overall spectral class must be about B, so that the calibration factor will be close to unity. The phase was calculated from the ephemeris of Belton and Woolf (1965),

$$\text{Primary minimum} = \text{JD } 2433289.47 + 12.92848E + 0.3556 \times 10^{-5}E^2 - 0.648 \times 10^{-10}E^3 \pm 0^d.18. \quad (50)$$

At the same time as the polarimetric data were being taken, the light intensity meter on the polarimeter was used as a photometer and a light curve obtained. The photometric reference was the star, γ Lyr, which is of similar spectral class and mean magnitude to β Lyr. The polarization data are plotted in figure 4.5, the typical error being $\pm$ 0.1%, and the photometric data (β Lyr - γ Lyr) in figure 4.6, the typical error being $\pm$ 0.04 magnitude. The position angle has not been plotted as it was approximately constant at 157 $\pm$ 10°.

The two curves taken together show the increased polarization at primary eclipse which is primarily due to the considerable decrease in system light at this phase. Also shown is the small drop in polarization at secondary eclipse caused by the scattering material between the two stars being

partially occulted. Of course, at primary eclipse this material is also partially occulted but the decrease in total light more than compensates. The increase in polarization at primary eclipse is greater than that previously seen in the U, B, V spectral regions, and this will be discussed in the next chapter, particularly in relation to the recent work of Huang (1978).

4.4 Algol

Algol was observed throughout several cycles and not once did the net polarization exceed 0.2%. Thus, both the interstellar and intrinsic polarization must be very low, in agreement with the work of Rudy and Kemp (1978).

Table I Polarimetric observations of standard stars

Polarized stars

Star	Measured % P	True* % P	P true/P meas.	Measured θ°	True* θ°
ϕ Cas	2.47 ± 0.31	3.4 ± 0.1	1.4 ± 0.2	96 ± 4	94 ± 1
η Aql	1.14 ± 0.06	1.8 ± 0.1	1.6 ± 0.2	100 ± 4	93 ± 1
55 Cyg	2.64 ± 0.27	2.8 ± 0.1	1.1 ± 0.2	2 ± 3	3 ± 1
2H Cam	2.89 ± 0.22	3.5 ± 0.1	1.2 ± 0.1	118 ± 4	115 ± 1
HD 21389	3.21 ± 0.04	3.74± 0.05	1.2 ± 0.1	118 ± 7	------

Non polarized stars

Star	Measured % P
β Aql	0.14 ± 0.12
α Lyr	0.18 ± 0.12
α Boo	0.18 ± 0.03
($p < 0.01\%$)	

Spectral data on the polarized stars

Star	Spectral class	(B-V)
ϕ Cas	F0 Ia	+0.68
η Aql	F6-G2 Ib	+0.80
55 Cyg	B3 Ia	+0.40
2H Cam	B9 Ia	+0.40
HD 21389	A0 Ia	+0.59

* from Serkowski (1974), except for HD 21389 taken from Serkowski, Mathewson and Ford (1975).

Table II Polarimetric observations of ρCas and HD 217476

ρCas

JD 2443000 +	%P	θ°
366	1.37 ± 0.16	46 ± 6
367	1.62 ± 0.33	66 ± 10
376	1.36 ± 0.14	58 ± 5
388	1.25 ± 0.25	50 ± 10
395	1.67 ± 0.34	58 ± 10
467	1.36 ± 0.20	44 ± 7
510	1.47 ± 0.21	49 ± 7

HD 217476

JD 2443000 +	%P	θ°
367	2.87 ± 0.41	65 ± 7
376	3.24 ± 0.38	67 ± 6
388	2.80 ± 0.57	64 ± 10
467	3.28 ± 0.33	57 ± 5
510	3.24 ± 0.46	67 ± 7

Table III Polarimetric and photometric observations of β Lyrae

JD 2443000 +	Phase	p%	θ°	Δm(ref. γ Lyrae)
396.688	0.606	0.71	156	
413.653	0.918	0.80	152	-
631.767	0.789	0.72	153	0.00
631.785	0.790	0.75	147	0.08
632.793	0.868	0.78	170	0.18
632.822	0.870	0.78	161	0.21
633.779	0.944	0.74	164	0.34
633.792	0.945	1.10	157	0.33
633.822	0.948	0.88	160	0.43
633.830	0.948	1.05	155	0.39
633.873	0.952	0.81	150	0.41
636.804	0.179	0.73	153	0.06
638.774	0.331	0.76	159	0.05
638.801	0.333	0.81	154	0.07
638.820	0.334	0.87	160	0.08
646.753	0.948	1.32	166	0.43
646.799	0.951	1.08	155	0.39
646.808	0.952	1.15	156	0.37
646.836	0.954	1.04	161	0.43
647.778	0.027	1.59	160	0.92
647.836	0.032	1.39	155	0.90
648.790	0.105	0.96	151	0.60
648.823	0.108	1.14	156	0.56
652.778	0.414	0.81	153	0.19
653.772	0.491	0.55	157	0.35

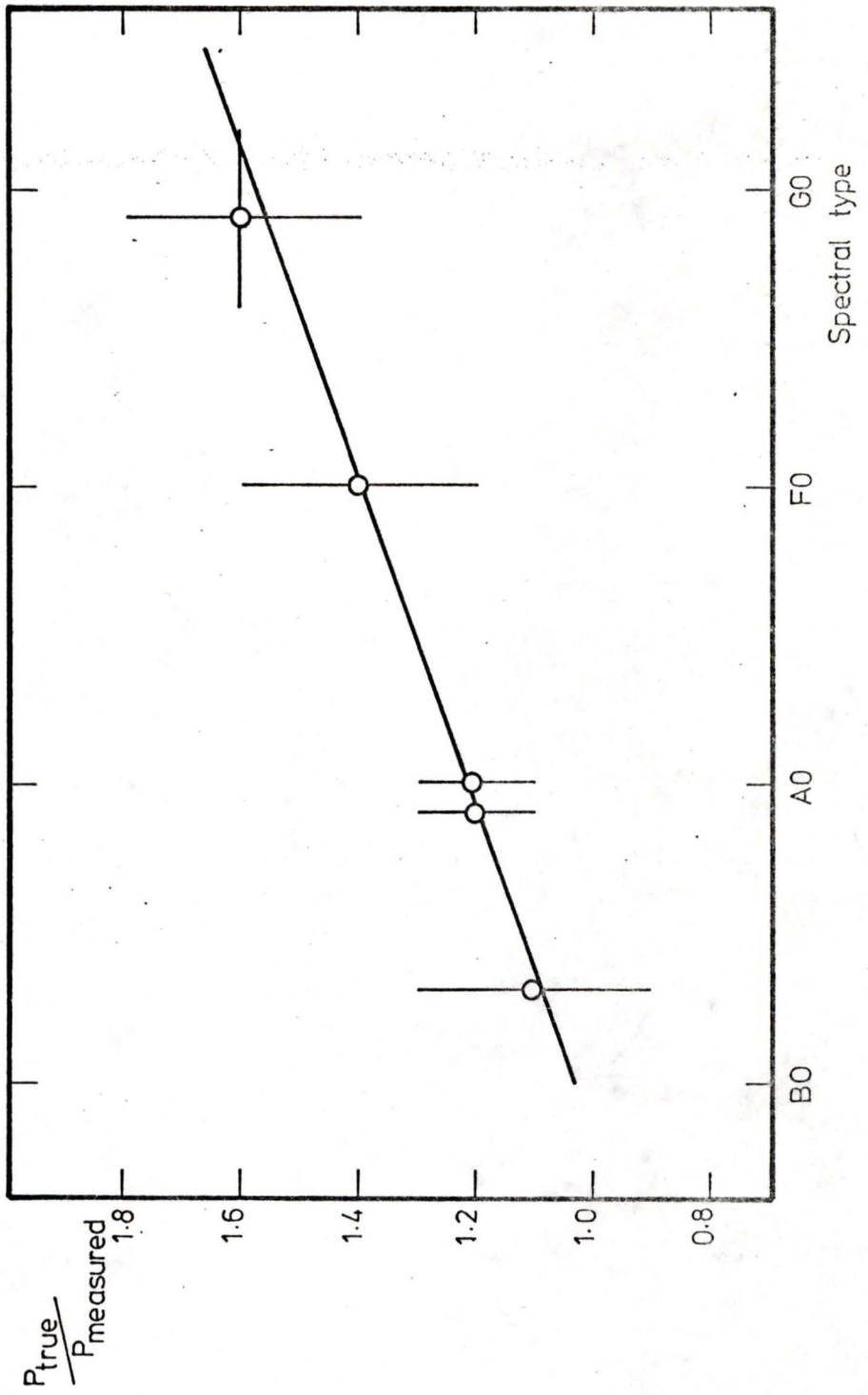

Fig. 4.1. $P_{true}/P_{measured}$ versus spectral type

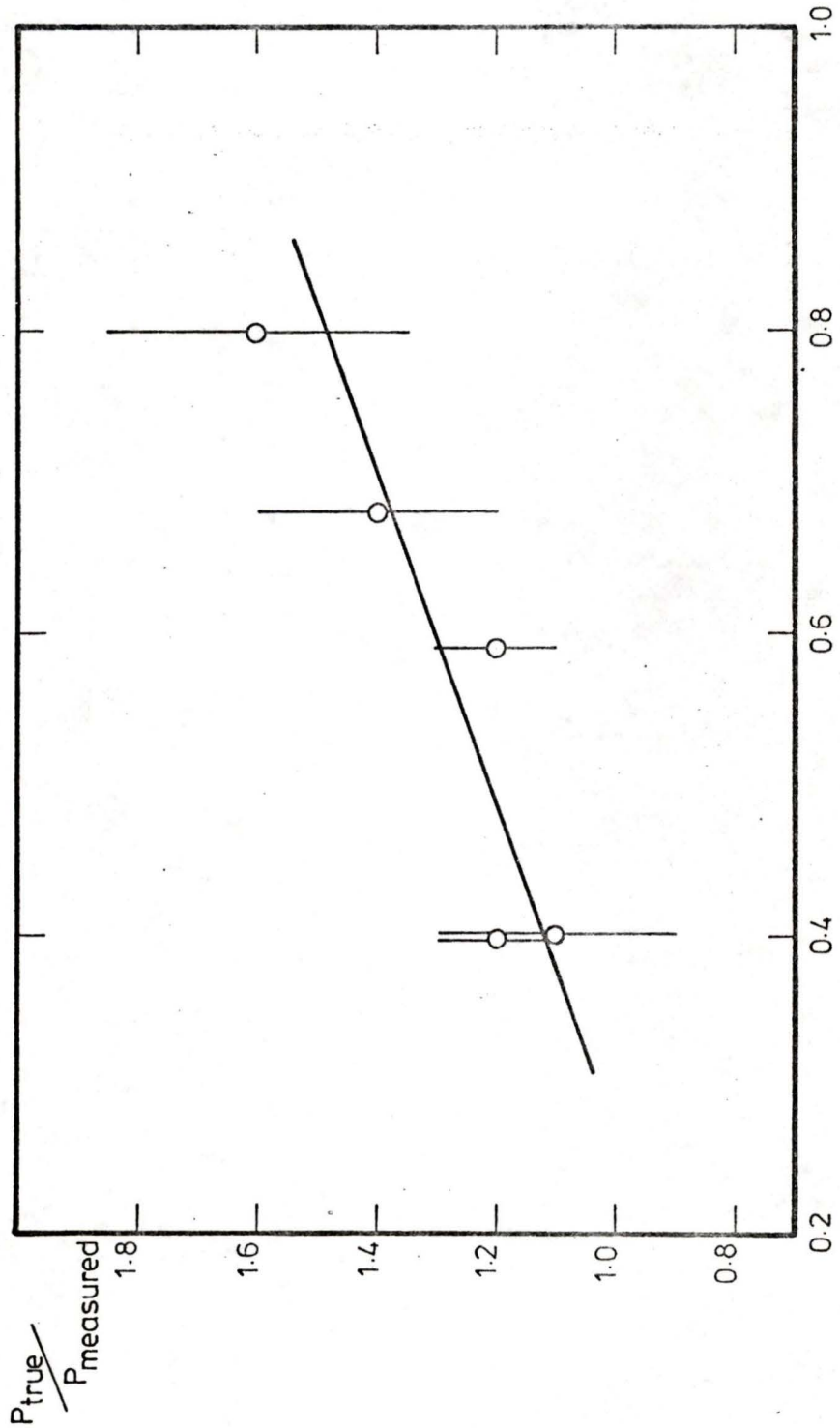

Fig. 4.2. $P_{true}/P_{measured}$ versus colour

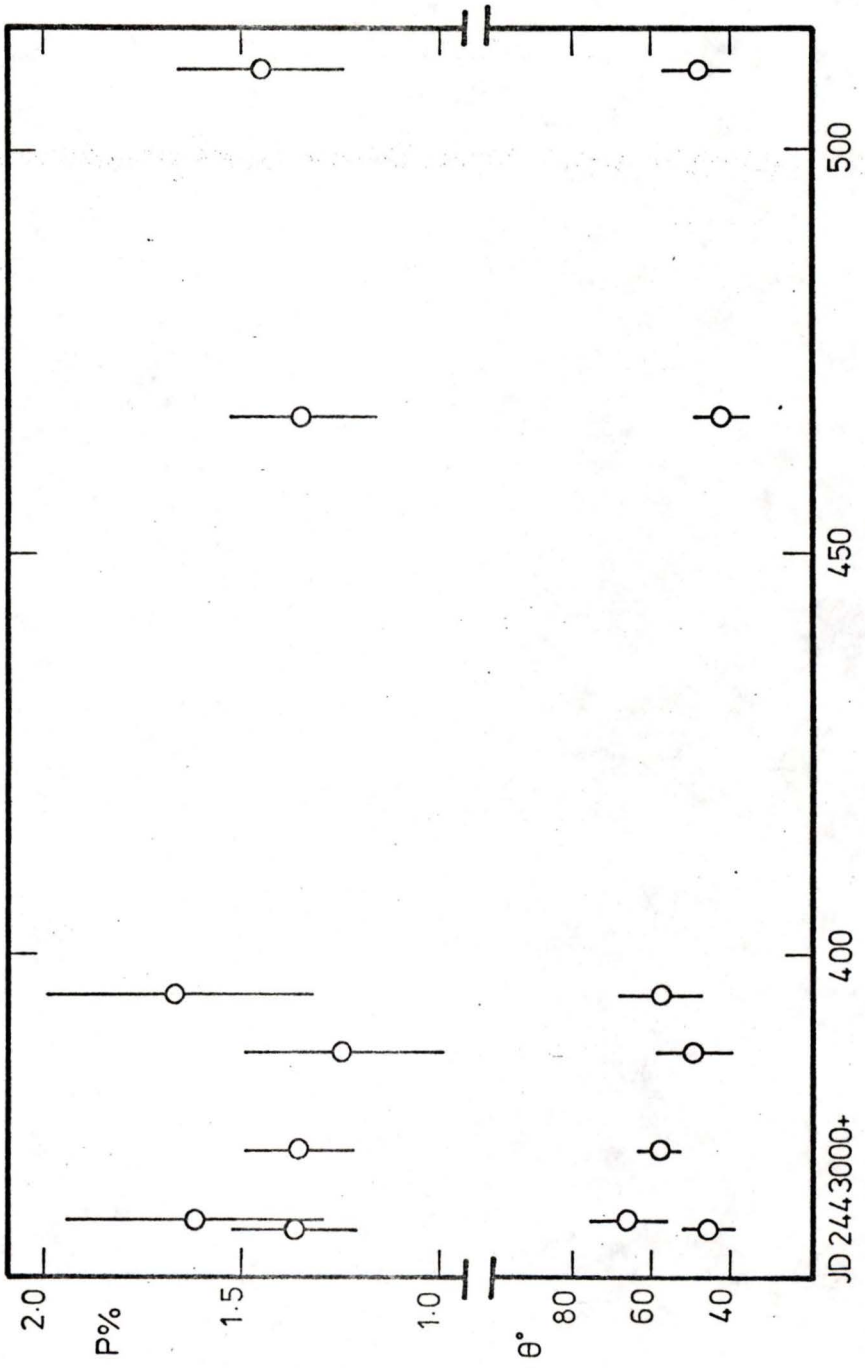

Fig.4.3. Polarimetric observations of ρ Cas

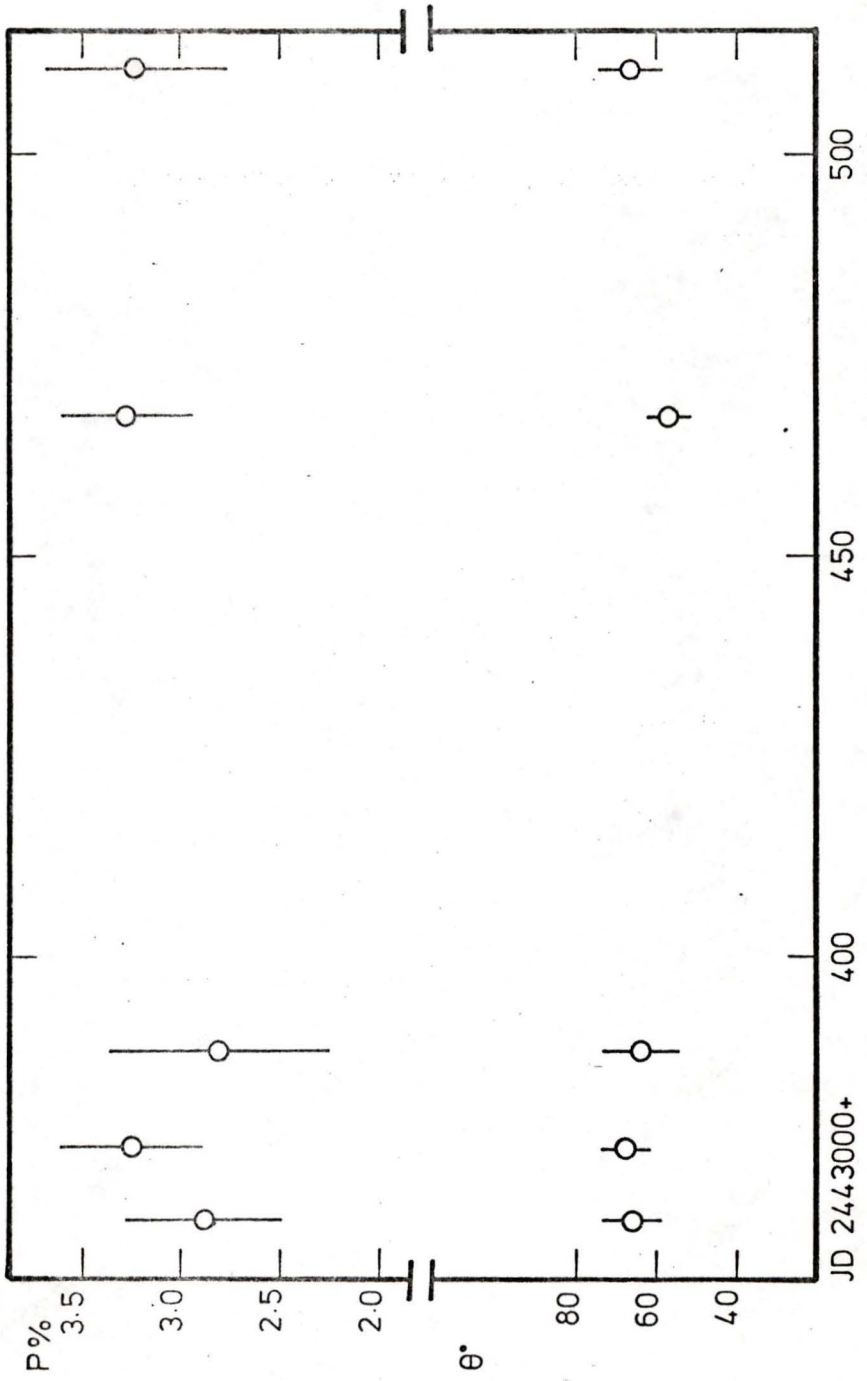

Fig. 4.4. Polarimetric observations of HD217476

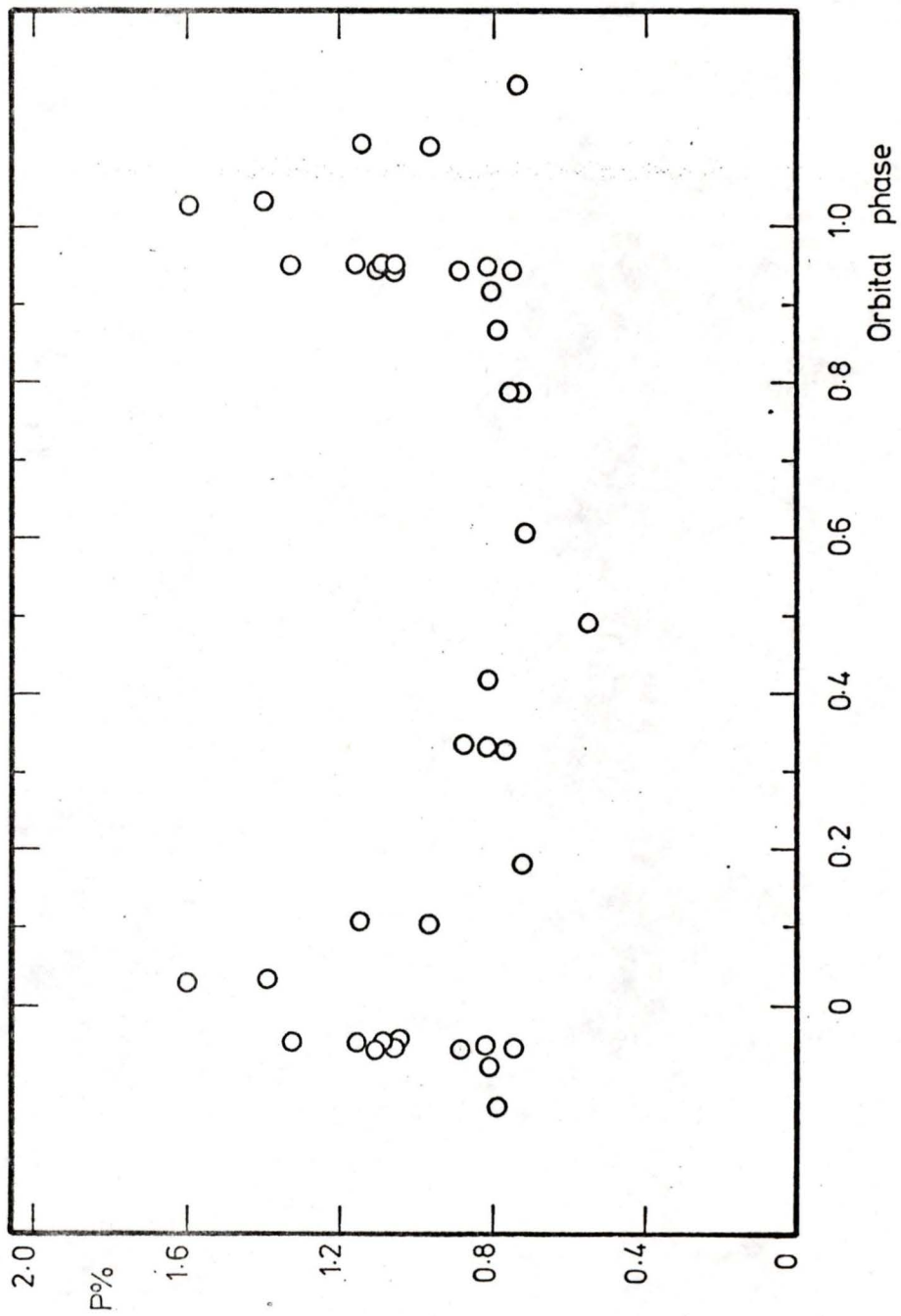

Fig. 4.5. Polarimetric observations of βLyr

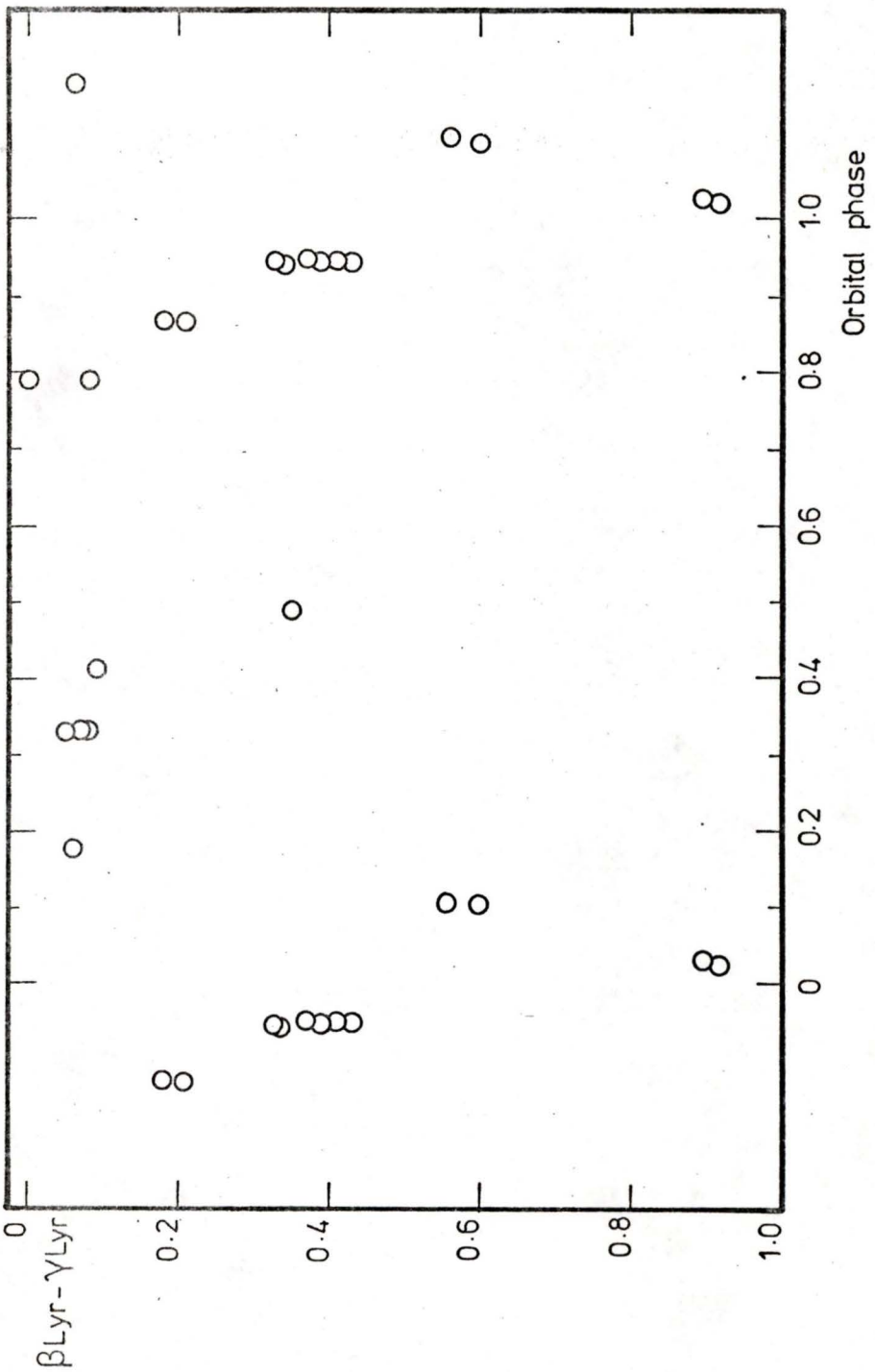

Fig. 4.6. Photometric observations of βLyr

CHAPTER 5 DISCUSSION AND CONCLUSIONS

The observational data presented in the previous chapter are now considered, particularly with relation to the published data of other observers.

5.1 The supergiant stars

According to Smolinski and Climenhaga (1978) and Humphreys and Ney (1974) there is some evidence that suggests that the supergiant stars, 89 Herculis, Rho Cassiopeiae and HD 217476 are probably all long period binaries. During several observing runs at the Dominion Astrophysical Observatory all three stars were observed to have emission lines, non-periodic variations in radial velocity and the spectral appearance of two superposed individual stellar spectra. There is some weak evidence of a 70 day period for 89 Herculis (Böhm-Vitense, 1956); this will be considered shortly.

An isolated star which is not rotating too rapidly should lose mass equally in all directions so that the stellar symmetry will be maintained and the integrated light will be unpolarized. However, if the mass-losing star is a member of a binary system, a good deal of the matter will be concentrated towards the orbital plane and may form an accretion disk around one of the stars. As was shown

in Chapter 2, this would lead to a net linear polarization of the system light. Binary nature should be revealed as a change in the polarization, phase locked to the orbital period. Interstellar polarization would dilute this effect to some extent. The three supergiant stars have therefore been monitored over a period of about a year to see if there is a significant change in polarization

5.1.1 89 Herculis

This star was found to be unpolarized over the whole observing period. Furthermore, this star has never been reported elsewhere as being polarized. While the observations do not provide support for 89 Herculis being a binary having substantial mass transfer (i.e. 10^{-6} solar mass per year), 89 Herculis could still be a binary but with a small mass transfer rate.

There is, in fact, evidence for significant mass loss in the form of spectroscopic and radial velocity changes found by several workers at Lick Observatory including Böhm-Vitense (1956), and by Climenhaga and Smolinski (1978). During a study of the hydrogen lines, $H\beta$ and $H\gamma$, Böhm-Vitense found radial velocity variations of some 20 km s^{-1}. There was very weak evidence for a 70 - 72 day period which is supported to some extent by the photometry of Worley (1956). He found

a 0.1 magnitude variablity in 89 Her that may have a period of about 70 days. However, as the photometric observations were close to the instrumental accuracy limit of the time, the 70 day period must be considered speculative, particularly in view of the lack of subsequent confirming observations.

On the above evidence, 89 Her is possibly a 70 day binary, but more likely a single star exhibiting variable mass loss.

5.1.2. Rho Cassiopeiae

Of the three supergiant stars, Rho Cassiopeiae has been studied the most extensively. As recently pointed out by Bailey (1978), this star has been known to be an irregular variable since 1900, and is classified (Kukarkin et al., 1970) as F8IaP,RCB?, partly because of a dip in visible light of some two magnitudes in September, 1946. Since 1946, ρCas has behaved as a semiregular variable with a cycle length of around 200 to 400 days. This can be seen from figure 5.1, which shows thirty day mean visual magnitudes for the period 1964 - 1975 (Bailey, 1978).

During the present observing period, there has been no significant change in linear polarization. Furthermore, this star has been observed on two previous occasions (see table IV) with results essentially the same as those reported here.

Serkowski et al. (1975) put ρCas (and also HD 217476) in their list of stars exhibiting interstellar polarization on this basis of five band polarimetry. The mean observed polarization for ρCas and HD217476 is plotted in figure 5.2 together with that for four of the standard stars in the current programme. The length and orientation of the bars represent the degree of polarization and the orientation of the plane of polarization, respectively. It should be pointed out that on the scale of this figure, the differences between the current observations and those reported elsewhere are undetectable. The most obvious feature is a 45° polarization vector rotation in the Cassiopeia region, which indicates that either the polarization is interstellar and the interstellar magnetic field undergoes a 45° twist, or we are seeing interstellar polarization superposed on a vector rotation intrinsic to the stars. Serkowski (1974) studied three of the standards, 55 Cyg, 2H Cam and ϕCas, with a spectropolarimeter and showed that the changes in polarization with wavelength are typical of interstellar polarization. This twist occurs at galactic longitude 115° which is where Mathewson and Ford's plot of galactic polarization (figure 2.1) shows a loss of parallelism with the galactic equator.

Finally, evidence of a circumstellar shell has been published by various observers. From a study of high disperison spectra taken between 1955 and 1960, Sargent (1961) found evidence of a circumstellar shell expanding at 40 Kms^{-1} relative to the photosphere. He

found emission lines of Fe I, Ni I and Ca I, whose variable strength he attributed to variations in the density of the shell. A curve of growth analysis gave a mean mass loss of 2×10^{-5} solar masses per year, which, however, varied sporadically over a range of about ten. Large differences in the shell appeared to take some 260 - 300 days to fully develop, in fair agreement with Bailey's photometric cycle length of 200 - 400 days. More recently, Joshi and Rautela (1978) have compared the continuous energy distribution of ρCas in the wavelength range 340 - 710 nm. with that of δCMa, said by Sargent (1961) to have the same photospheric spectrum as ρCas apart from the circumstellar feature of the latter. They found the flux from ρCas at wavelengths shorter than 410 nm. to be greater than that from δCMa, and to be variable on the scale of days. They suggest that this excess flux may be attributed to hydrogen emission in the associated chromosphere of the star, the variability being due to short duration heating bursts. More importantly for this discussion is their observation that the Paschen continuum of ρCas had a different and variable slope compared with that of δCMa. The variability was greatest around 700 nm. consistent with a circumstellar shell cooler than the central star and fluctuating in density.

It thus appears that all observations are consistent with a variable circumstellar shell around ρCas, and there is no need to invoke binary nature.

5.1.3 HD 217476

Polarimetric observations of this star are similar to those of ρ Cas in that the present observations show no short term changes, and comparison with previous work (see table IV) shows no statistically significant long term changes. Furthermore, spectropolarimetry (Serkowski et al., 1970) suggests an interstellar origin for the polarization. The observations of Smolinski (1977) can be interpreted as mass loss, but as they have not yet been published, the actual rate of mass loss is difficult to determine. If it were significant, the constancy of the polarization would argue against HD 217476's being a binary.

It is therefore only correct to say that the polarimetric data offer no definite evidence for or against the possible binary nature of HD 217476.

5.2 Beta Lyrae

The variations in the linear polarization of the light from Beta Lyrae have been studied over the past sixteen years by many observers. Figure 5.3 shows the V-band observations of Shakhovskoi (1965) together with his predicted polarization curve. The present observations, shown in figure 4.5, show the same general change with orbital phase. The out of eclipse mean polarizations are essentially the same, whereas the rise at primary eclipse is larger in this work, 1.5% as compared to 0.9%. The most likely reason for this difference is the two wavebands used; the present polarimeter has an optical passband of approximately 475 - 725 nm. whereas Shakhovskoi's results were obtained using the Johnson V-band, i.e. approximately 500 - 575 nm. This 'wavelength effect' has been noticed before (e.g. Rucinski, 1966; Coyne, 1970) primarily in the U, B, V bands, where the polarization at primary eclipse is greater going to longer wavelengths.

From the present results, this trend appears to continue into the red and near infra-red with ever increasing levels of polarization. Coyne (1970) did make some measurements showing the polarization levelling off at about 550 nm. and then falling slowly at longer wavelengths. However, his 500 nm. results differ considerably from those of other observers. Furthermore, he used non-standard but unspecified wavelength bands, so that his results are difficult to interpret. The usual

explanation for the drop in polarization at short wavelengths is increased absorption in the circumstellar envelope which causes depolarization through multiple scattering.

Recently Huang (1978) has studied the changes in H_α and H_γ line profiles with the orbital phase of Beta Lyrae. In particular he studied the change with orbital phase of the difference between the radial velocities in emission and absorption. The change was much greater for H_α than for H_γ. He assumed that the emission feature of a particular line is generated a little further out in the circumstellar shell than is the absorption feature so that the change in emission-to-absorption velocity difference is a function of the local gas flow velocity gradient. Huang concluded that the H_γ line must be generated near to the secondary companion so as to share its radial velocity changes, whereas H_α originates in the gaseous medium enveloping the entire system, thus showing very little change in velocity difference over the orbital period. It is not known whether this spatial differentiation holds also for the continuum radiation, although the present work suggests that it might.

From the light curve of figure 4.6, it can be seen that the increase in polarization by a factor of about two at primary eclipse is accompanied by a 50% decrease in the system light. Now if this broad band polarization is produced in that part of the envelope surrounding both stars the product of system light and degree of polarization should be constant.

The observed increase in polarization is then just a consequence of the increasing ratio of polarized to non-polarized light. However, if the polarization were produced in the vicinity of the secondary companion, some of the polarized flux would be eclipsed with the primary star, so that the increase in polarization would not be as great as the decrease in light. This is exactly what is observed for the V-band data and supports the theory that the increase in polarization at primary eclipse is larger than Shakhovskòi's simply because of the difference in wavelength region studied. Furthermore, the red scattered flux appears to come from that part of the envelope surrounding both stars, whereas the blue flux comes from the vicinity of the secondary companion.

5.3 Algol

The linear polarization of Algol remained below the threshold detection limit of 0.2% throughout the orbital cycle. This agrees with the recent observations of Rudy and Kemp (1978) shown here in figure 5.4. Their data, obtained with a more sensitive polarimeter, show phase-locked changes in polarization, but at all times below the 0.03% level*. The amount of scattering material in the system is obviously at least an order of magnitude less than that in β Lyr, as has been known for some time from photometry.

* Note that both U and Q values separated by 0.5 phase are similar, so that a Q,U plot would be a degenerate ellipse, as described previously in Chapter 2.

5.4 Further work

It has become apparent during this work that a more sensitive instrument possessing a lower instrumental polarization is essential for further observations. Cooling the present silicon diode/preamplifier combination would increase the sensitivity by at least an order of magnitude but would not lower the instrumental polarization; this would require a different modulator/analyzer. A system similar to that built by Stokes et al., (1976), and described previously in Chapter 3.2 (figure 3.3) is probably the best choice from the standpoint of both high sensitivity and low instrumental polarization.

As for observations, a new spectropolarimeter, similar to that of Stokes et al. (1976), and currently in operation at the Royal Observatory Edinburgh, will be used by the author to look for the possible 70 day period of 89 Herculis, and to check the wavelength dependence of polarization in Beta Lyrae.

Table IV Past and present observations of ρCas and HD 217476

ρCas

%P	θ°	Source
1.47 ± 0.04	55	Coyne et al. (1974)
1.41 ± 0.06	55 ± 1	Serkowski (1965)
1.44 ± 0.15	53 ± 8	Present work

HD 217476

%P	θ°	Source
2.86 ± 0.04	71	Kruszewski (1962)
2.82 ± 0.30	71	Treanor (1963)
2.80 ± 0.13	-	Serkowski (1968)
2.70 ± 0.36	12	Coyne et al. (1974)
3.09 ± 0.23	64 ± 4	Present work

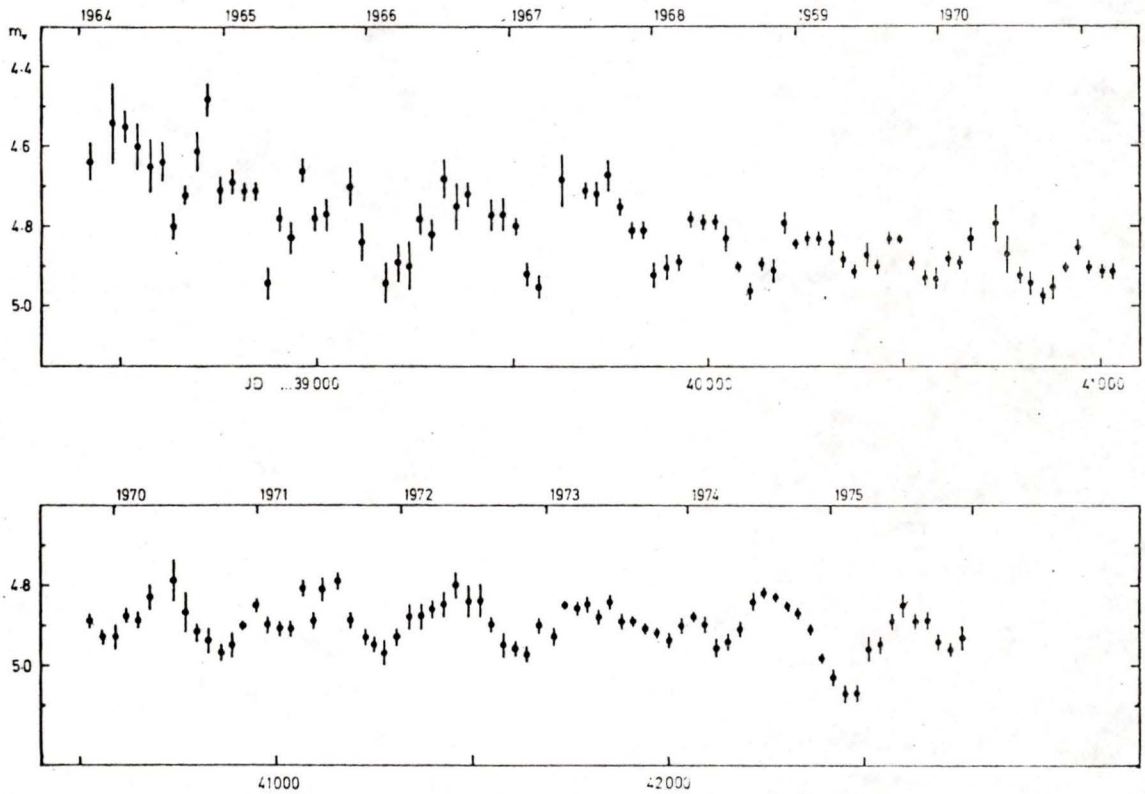

Fig. 5.1 Thirty-day means of observations of Rho Cassiopeiae. Bars indicate ±1 s.e.
(Reproduced with permission from J. Brit. Astr. Assoc., 88, 399)

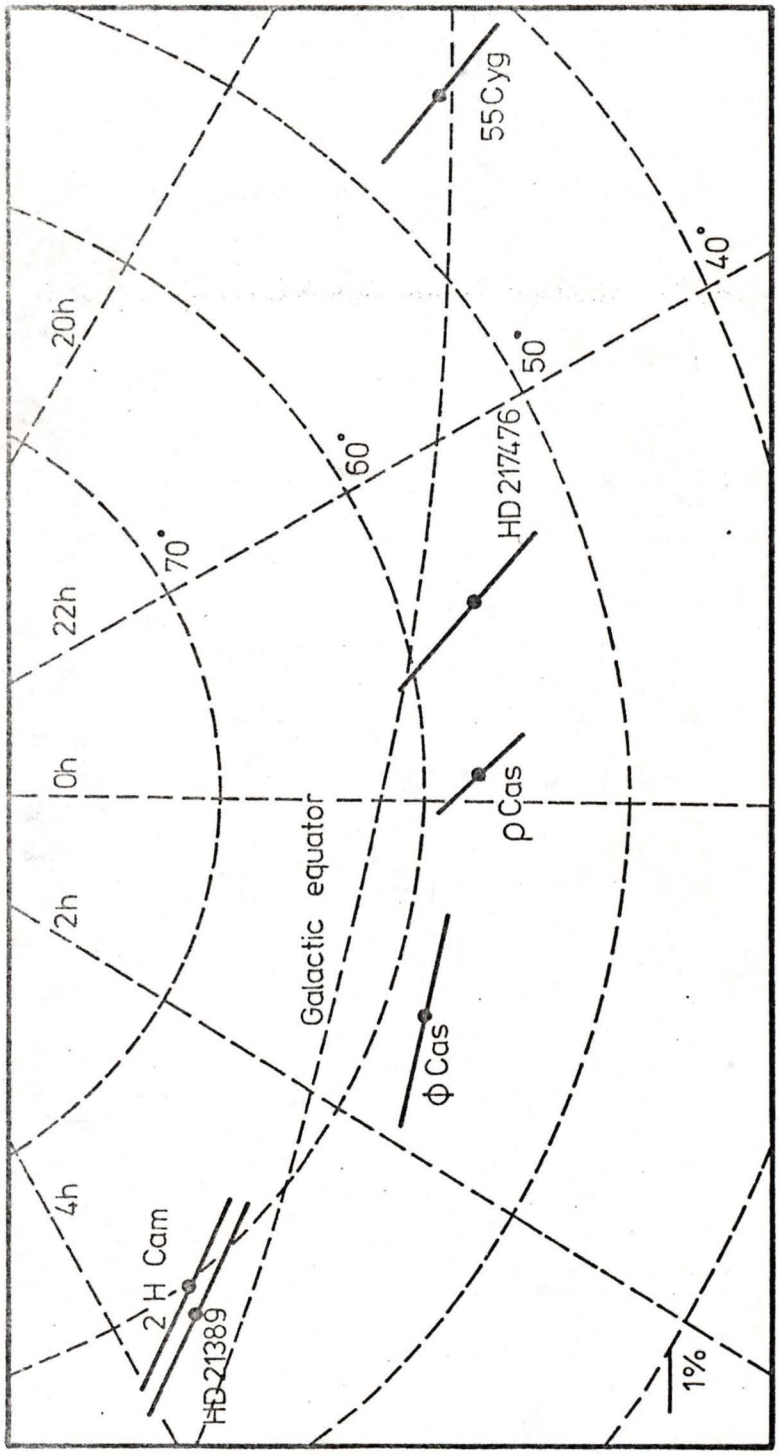

Fig. 5.2. Galactic orientation of polarization vectors

(a)

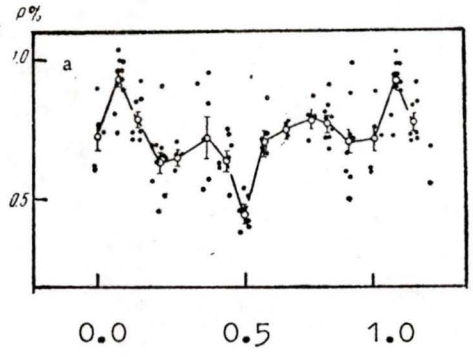

(b)

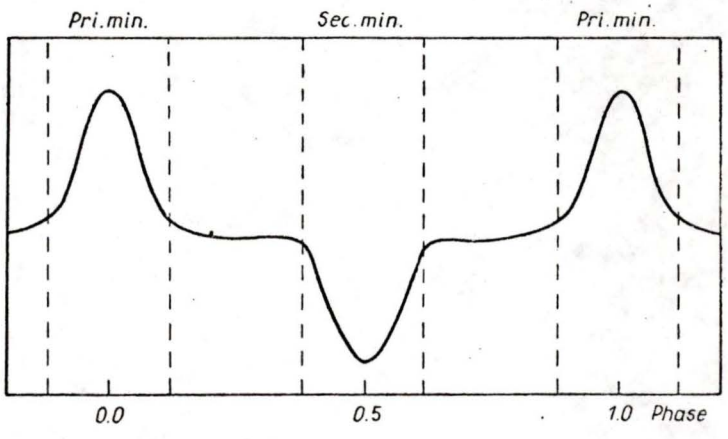

Fig. 5.3 Shakhovskoi's observed (a) and modelled (b) polarization curves for Beta Lyrae.
(Reproduced with permission from Soviet Astronomy, 8, 835.)

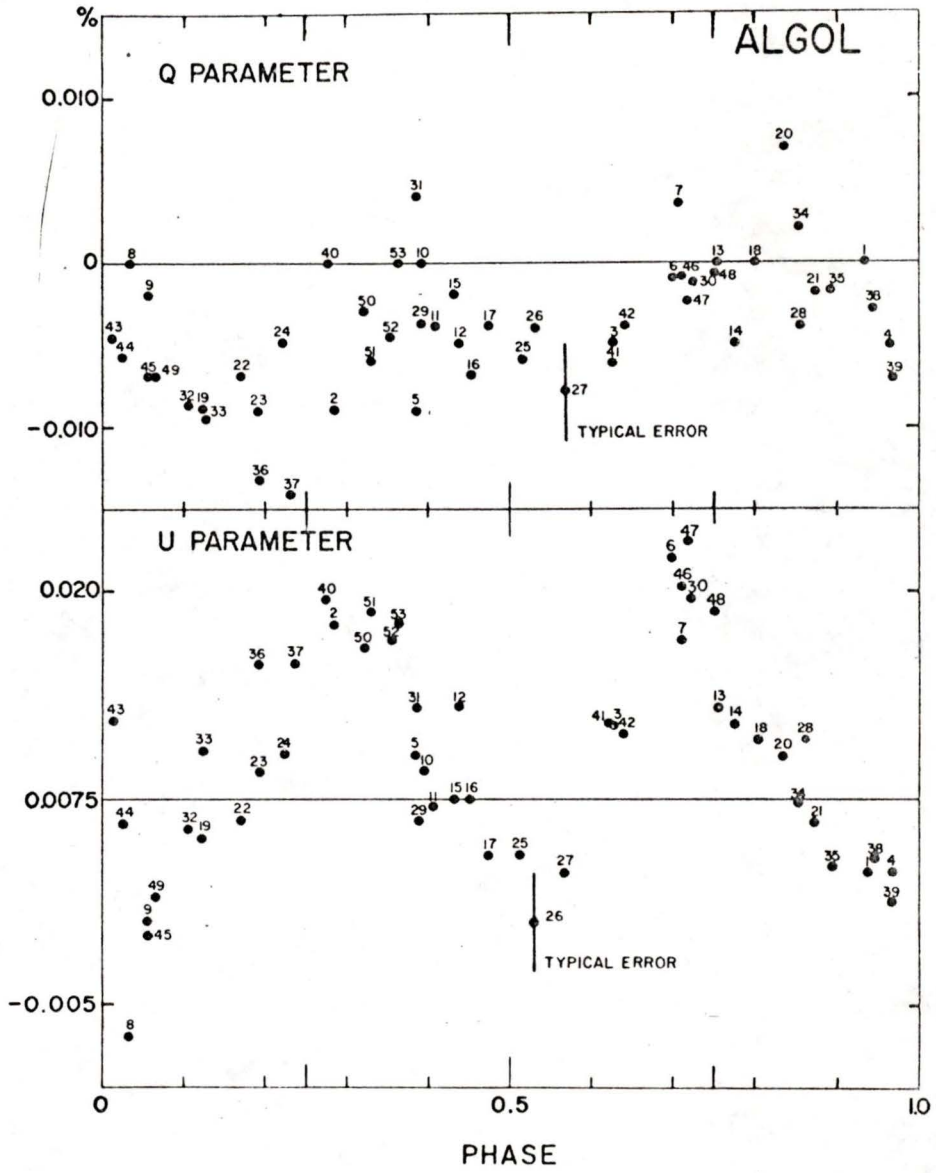

Fig. 5.4 Rudy and Kemp's polarimetric observations of Algol, plotted against the 2.87 day period. Observations are in the B filter.
(Reproduced with permission from Ap. J., 221, 205.)

BIBLIOGRAPHY

Angel, J.R.P., and Landstreet, J.D. (1970), Ap. J., 160, L148.

Bailey, J. (1978), J. Brit. Astr. Assoc., 88, 397.

Belton, M.J.S., and Woolf, N.J. (1965), Ap. J., 141, 145.

Bohm-Vitense, E. (1956), Pub. A.S.P., 68, 57.

Chandrasekhar, S. (1946), Ap. J., 103, 351.

Clarke, D., and McLean, I.S. (1975), M.N.R.A.S., 172, 545.

Climenhaga, J.L., and Smolinski, J. (1978), private communication.

Coyne, G.V. (1970), Ap. J., 161, 1011.

Coyne, G.V. (1974), in "Planets, Stars and Nebulae studied with photo-polarimetry", ed. T. Gehrels, U. Arizona Press, p. 888.

Coyne, G.V., Gehrels, T., and Serkowski, K. (1974), Astr. J., 79, 581.

Davis, L., and Greenstein, J.L. (1951), Ap. J., 114, 206.

Dolan, J.F. (1976), in "X-ray Binaries", proceedings of NASA symposium, NASA SP-389, Greenbelt, Maryland, p. 493.

Hall, J.S. (1949), Science, 109, 166.

Hiltner, W.A. (1949), Science, 109, 165.

Hiltner, W.A. (1956a), Ap. J. Suppl., 2, 389.

Hiltner, W.A. (1956b), Vistas in Ast., 2, 1086.

Huang, S.-S. (1978), Ap. J., 222, 627.

Humphreys, R.M., and Ney, E.P. (1974), Ap. J., 190, 339.

Joshi, S.C., and Rautela, B.S. (1978), M.N.R.A.S., 183, 55.

Kemp, J.C. (1969), J. Optical Soc. Amer., 59, 950.

Kemp, J.C., and Wolstencroft, R.D. (1973), Ap. J., 179, L33.

Kruszewski, A. (1962), Pub. A.S.P., 74, 519.

Kukarkin, B.V. et al., (1970), General Catalogue of Variable Stars, 3rd Edition, Moscow.

Landstreet, J.D. (1974), in "Planets, Stars and Nebulae studied with photopolarimetry", ed. T. Gehrels, U. Arizona Press, p. 981.

Mathewson, D.S., and Ford, V.L. (1970), Memoirs R.A.S., 74, 139.

Piirola, V. (1975), I.A.U. Commission 27, 1061.

Purcell, E.M. (1975), in "The Dusty Universe" ed. G.B. Field and A.G.W. Cameron, Neale Watson Academic Publications, New York, p. 155.

Rucinski, S.M. (1966), Acta Astronomica, 16, 127.

Rudy, R.J. (1977), Ph.D. Thesis, U. of Oregon.

Rudy, R.J., and Kemp, J.C. (1976), Ap. J., 207, L125.

Rudy, R.J., and Kemp, J.C. (1978), Ap. J., 221, 200.

Sargent, W.L.W. (1961), Ap. J., 134, 142.

Serkowski, K. (1965), Ap. J., 141, 1340.

Serkowski, K. (1968), Ap. J., 154, 115.

Serkowski, K. (1974), in "Planets, Stars and Nebulae studied with photo-polarimetry", ed. T. Gehrels, U. Arizona Press, p. 135.

Serkowski, K., Mathewson, D.S., and Ford, V.L. (1975), Ap. J., 196, 261.

Shakhovskoi, N.M. (1962), Soviet Astr., 6, 587.

Shakhovskoi, N.M. (1965), Soviet Astr., 8, 833.

Smolinski, J. (1977), private communication.

Stokes, R.A., Ekstrom, P.A., and Swedland, J.B. (1976), Optical Engineering, 15, 7.

Treanor, P.J. (1963), Astr. J., 68, 185.

Worley, C.E., (1956), Pub. A.S.P., 68, 62.

APPENDIX A

DERIVATION OF THE VALUES OF Q AND U PRODUCED BY A NON-UNIFORM DISTRIBUTION OF SCATTERERS (following Rudy, 1977)

Consider the geometry of the system shown in figure A.1. An individual scatterer is situated in a fixed position with respect to the stars. A coordinate system is centred at the scatterer with a fixed orientation relative to the scatterer. If $\hat{s}$ and $\hat{o}$ represent unit vectors directed from the scatterer to star #1 and to the observer, respectively, then the scattering angle, Ψ , is given by:

$$\cos\Psi = \hat{s}.\hat{o} = \sin i \sin 2\pi\alpha \sin 2\pi\alpha_1 + \sin i \cos 2\pi\alpha \cos 2\pi\alpha_1$$

$$= \sin i \cos 2\pi(\alpha - \alpha_1) \qquad (51)$$

From this, the fractional polarization of the scattered light is given by:

$$p = \frac{1 - \cos^2\Psi}{1 + \cos^2\Psi} = \frac{1 - \sin^2 i \cos^2 2\pi(\alpha - \alpha_1)}{1 + \sin^2 i \cos^2 2\pi(\alpha - \alpha_1)} \qquad (52)$$

The light incident on the scatterer from the star is assumed to be unpolarized. The factor 2π arises from the azimuthal angles being measured in units of orbital phase rather than in radians.

The polarization will be normal to the scattering plane. The unit vector in this direction, $\hat{n}$, is given by:

$$\hat{n} = \frac{\hat{s} \times \hat{o}}{|\hat{s} \times \hat{o}|}$$

$$= \frac{-\cos i \cos 2\pi\alpha_1,\ \cos i \sin 2\pi\alpha_1,\ \sin i \sin 2\pi(\alpha - \alpha_1)}{\left[1 - \sin^2 i \cos^2 2\pi(\alpha - \alpha_1)\right]^{\frac{1}{2}}} \qquad (53)$$

The normal to the scattering plane is perpendicular to the direction of the observer and lies in the Q', U' plane. The direction of Q' is in the polar direction. If the angle between a unit vector, $\hat{q}$, directed along Q', and the unit vector, $\hat{n}$, is denoted by β, then the values for Q' and U' are the projections of the fractional polarization, p, on the Q', U' axes.

$$Q' = p \cos 2\beta \ , \quad U' = p \sin 2\beta \qquad (54)$$

The value of $\cos\beta$ is found from:

$$\begin{aligned} \cos\beta &= \hat{q} \cdot \hat{n} \\ &= (-\cos i \sin 2\pi\alpha, -\cos i \cos 2\pi\alpha, \sin i) \cdot \\ &\quad \frac{\left[-\cos i \cos 2\pi\alpha_1,\ \cos i \sin 2\pi\alpha_1,\ \sin i \sin 2\pi(\alpha - \alpha_1)\right]}{\left[1 - \sin^2 i \cos^2 2\pi(\alpha - \alpha_1)\right]^{\frac{1}{2}}} \end{aligned} \qquad (55)$$

From this, $\cos 2\beta$ and $\sin 2\beta$ are found:

$$\cos 2\beta = \frac{\sin 2\pi(\alpha - \alpha_1) - \cos^2 i \cos^2 2\pi(\alpha - \alpha_1)}{1 - \sin^2 i \cos^2 2\pi(\alpha - \alpha_1)} \qquad (56)$$

$$\sin 2\beta = \frac{\cos i \sin 4\pi(\alpha - \alpha_1)}{1 - \sin^2 i \cos^2 2\pi(\alpha - \alpha_1)} \qquad (57)$$

Multiplying both expressions by p, equation (52), yields Q' and U'

$$Q' = \frac{\sin^2 2\pi(\alpha - \alpha_1) - \cos^2 i \cos 2\pi(\alpha - \alpha_1)}{1 + \sin^2 i \cos^2 2\pi(\alpha - \alpha_1)} \qquad (58)$$

$$U' = \frac{\cos i \sin 4\pi(\alpha - \alpha_1)}{1 + \sin^2 i \cos^2 2\pi(\alpha - \alpha_1)} \qquad (59)$$

A similar expansion is obtained for the other star in the system by replacing α_1 by α_2. Because of the additive nature of the Stokes parameters, the total Q' and U' are the sums of the individual Q' and U' values. However, before this is done, the individual Q', U' pairs need to be multiplied by an additional factor, $B_{1,2}$, which takes account of the finite size of the two stars and the relative contributions of scattered light from the two stars. The explicit form of B_1 is:

$$B_1 = \frac{\Phi_1}{\Phi_1 + \Phi_2} \cdot \frac{2\pi - \Omega_1}{2\pi} \tag{60}$$

where Φ_1 is the scattered flux which is incident from star #1, and Ω_1 is the solid angle subtended by star #1 at the scatterer. Hence, we may define

$$Q'_1 = \frac{B_1 \left[\sin^2 2\pi(\alpha - \alpha_1) - \cos^2 i \cos^2 2\pi(\alpha - \alpha_1) \right]}{1 + \sin^2 i \cos^2 2\pi(\alpha - \alpha_1)} \tag{61}$$

$$U'_1 = \frac{B_1 \left[\cos i \sin 4\pi(\alpha - \alpha_1) \right]}{1 + \sin^2 i \cos^2 2\pi(\alpha - \alpha_1)} \tag{62}$$

The scatterer cannot be resolved from the two stars so that the observable quantities are the ratios of Stokes parameters to the total system flux. As the total flux is much greater than the scattered flux, the observable parameters are:

$$Q_1 = \frac{A_1 \left[\sin^2 2\pi(\alpha - \alpha_1) - \cos^2 i \cos^2 2\pi(\alpha - \alpha_1) \right]}{\Phi_o} \tag{63}$$

$$U_1 = \frac{A_1 \left[\cos i \sin 4\pi(\alpha - \alpha_1) \right]}{\Phi_o} \tag{64}$$

where Φ_o is the total flux outside eclipse,

and A_1 equals $\Phi_1 \cdot \frac{(2\pi - \Omega_1)}{2\pi}$ to keep Q_1 and U_1 dimensionless.

For the case of a single scatterer illuminated by one star, $Q = Q_1$ and $U = U_1$. The dependence of Q and U on the orbital phase, α, can be eliminated by expressing Q in terms of $\cos 4\pi(\alpha - \alpha_1)$ and U in terms of $\sin 4\pi(\alpha - \alpha_1)$. Squaring both, adding them together and equating to unity yields:

$$\frac{\left[Q - (A_1/\Phi_o)\ \frac{\sin^2 i}{2}\right]^2}{\left[(1 + \cos^2 i)/2\right]^2} + \frac{U^2}{\cos^2 i} = \frac{A_1^2}{\Phi_o^2} \qquad (65)$$

This is the equation of the elliptical Q, U plot described previously in Chapter 2 for the case of a single scatterer.

For the more realistic case of a finite scattering region illuminated by both stars, it is necessary to sum the Stokes parameters for each individual scatterer, whereupon they take the form:

$$Q = \sum_{j=1}^{m} \left(\frac{\sin^2 i}{2} - \tfrac{1}{2}(1 + \cos^2 i) \cos 4\pi(\alpha - \alpha_{1j})\right) \frac{A_{1j}}{\Phi_o} + \sum_{j=1}^{m} \left(\frac{\sin^2 i}{2} - \tfrac{1}{2}(1 + \cos^2 i) \cos 4\pi(\alpha - \alpha_{2j})\right) \frac{A_{2j}}{\Phi_o} \qquad (66)$$

$$U = \sum_{j=1}^{m} \cos i \left(\frac{A_{1j}}{\Phi_o} \sin 4\pi(\alpha - \alpha_{1j}) + \frac{A_{2j}}{\Phi_o} \sin 4\pi(\alpha - \alpha_{2j})\right) \qquad (67)$$

where the subscript, j, refers to the individual scatterers of which there are a total of m.

The two equations, (66) and (67), may be simplified by using angle-difference formulae, and defining three new quantities:

$$m\,\bar{A} = \sum_{j=1}^{m} (A_{1j} + A_{2j}) \tag{68}$$

$$S_1 = \sum_{j=1}^{m} (A_{1j} \cos 4\pi\alpha_{1j} + A_{2j} \cos 4\pi\alpha_{2j}) \tag{69}$$

$$S_2 = \sum_{j=1}^{m} (A_{1j} \sin 4\pi\alpha_{1j} + A_{2j} \sin 4\pi\alpha_{2j}) \tag{70}$$

The quantities $S_{1,2}$ describe the distribution of scatterers such that for a uniform circumstellar disk, $S_1 = S_2 = o$, and $\bar{A}$ describes the mean illumination of each scatterer.

Then Q and U may be rewritten:

$$\frac{Q - (m\bar{A}/\Phi_o)\sin^2 i}{-\frac{1}{2}(1 + \cos^2 i)} = \frac{S_1}{\Phi_o} \cos 4\pi\alpha + \frac{S_2}{\Phi_o} \sin 4\pi\alpha \tag{71}$$

$$\frac{U}{\cos i} = \frac{S_1}{\Phi_o} \sin 4\pi\alpha - \frac{S_2}{\Phi_o} \cos 4\pi\alpha \tag{72}$$

Elimination of $\cos 4\pi\alpha$ and $\sin 4\pi\alpha$ by the usual technique leads to:

$$\left(\frac{Q - (m\bar{A}/\Phi_o)\sin^2 i}{\frac{1}{2}(1 + \cos^2 i)}\right)^2 + \frac{U^2}{\cos^2 i} = \frac{S_1^2 + S_2^2}{\Phi_o^2} \tag{73}$$

This is the equation of the elliptical Q,U plot described previously for the case of a finite scattering region.

It should be noted that Φ_o, the total system light flux is assumed constant.

Many binaries do not have a constant light output but suffer changes both in and out of eclipse. If the eclipse is of short duration and the out-of-eclipse variations are small, a Q, U plot can still be obtained. However, for systems such as Beta Lyrae in which the eclipses are broad and deep, Φ_o must be replaced by a series expansion. This is discussed further in Rudy (1977).

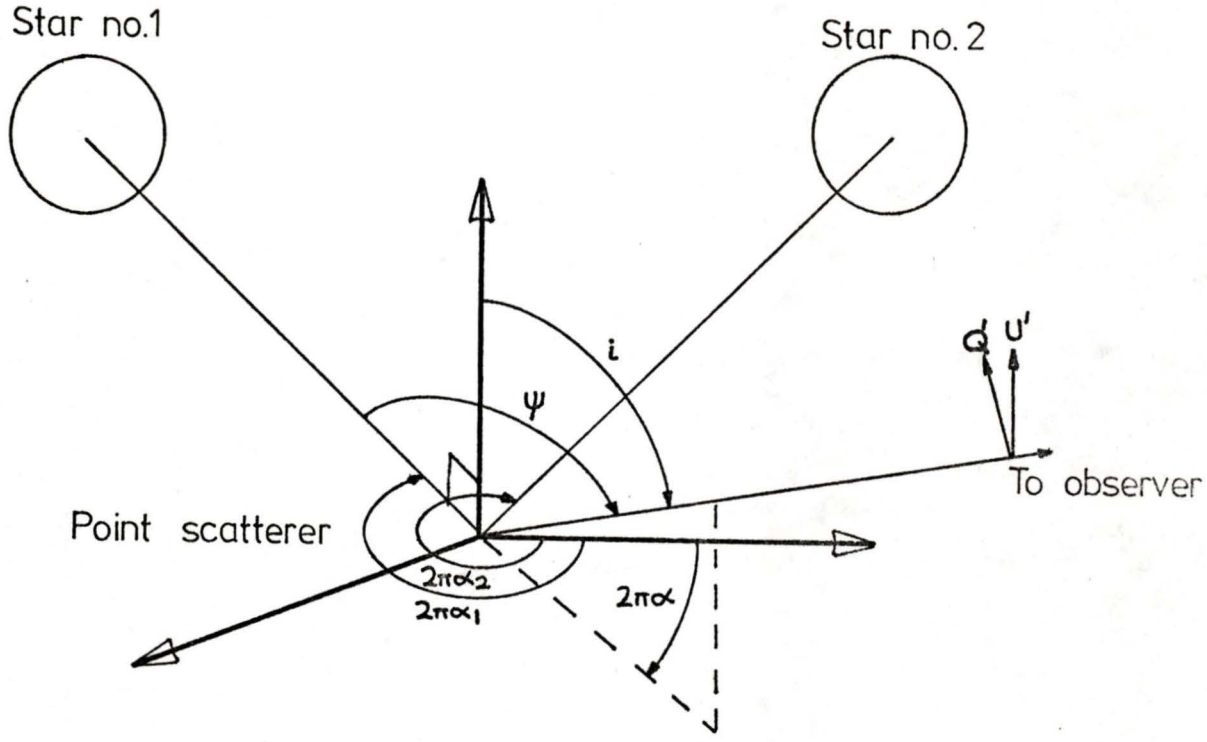

Fig. A.1. A schematic diagram of a point scatterer in the orbital plane of a binary system

APPENDIX B

CIRCUIT DIAGRAM OF EXISTING POLARIMETER

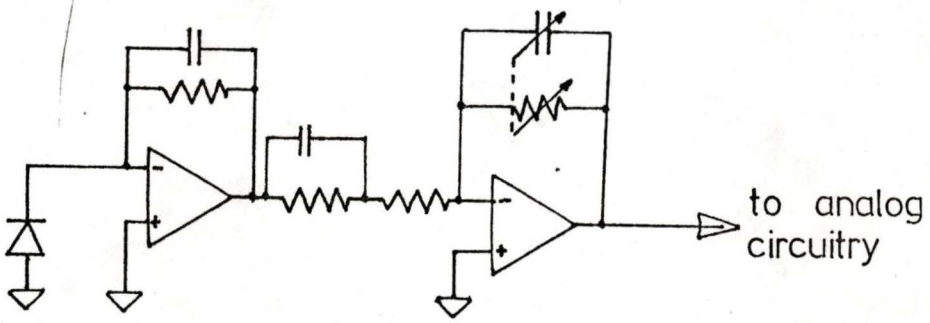

Head amplifier

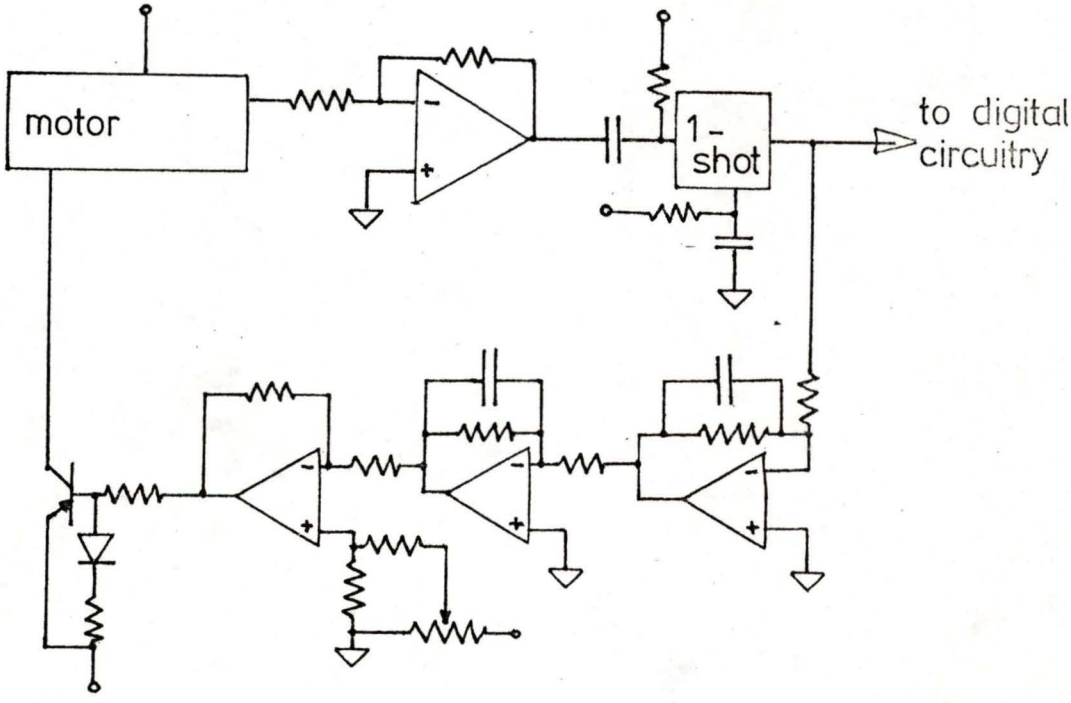

Motor speed controller

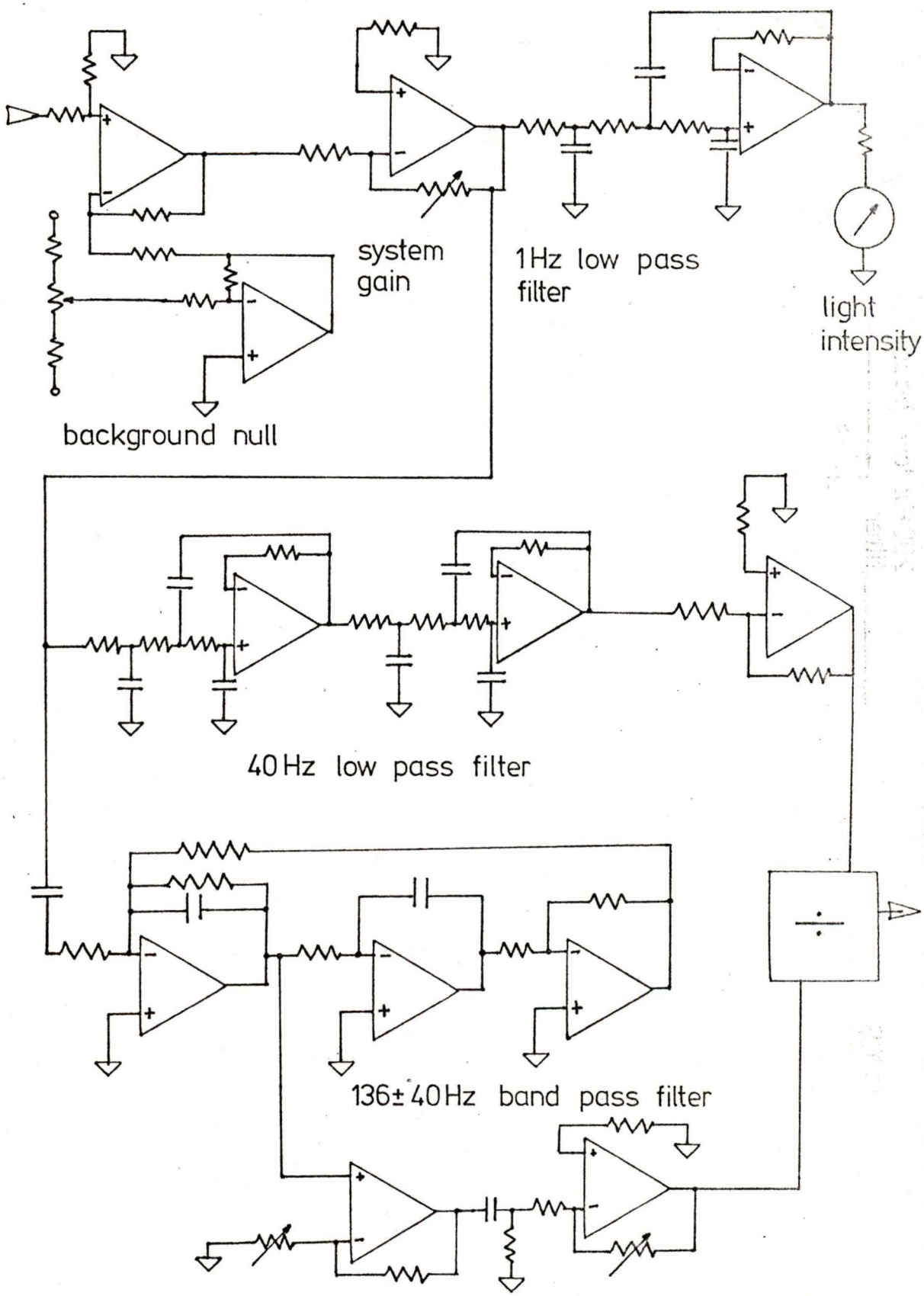

ANALOG SIGNAL PROCESSOR

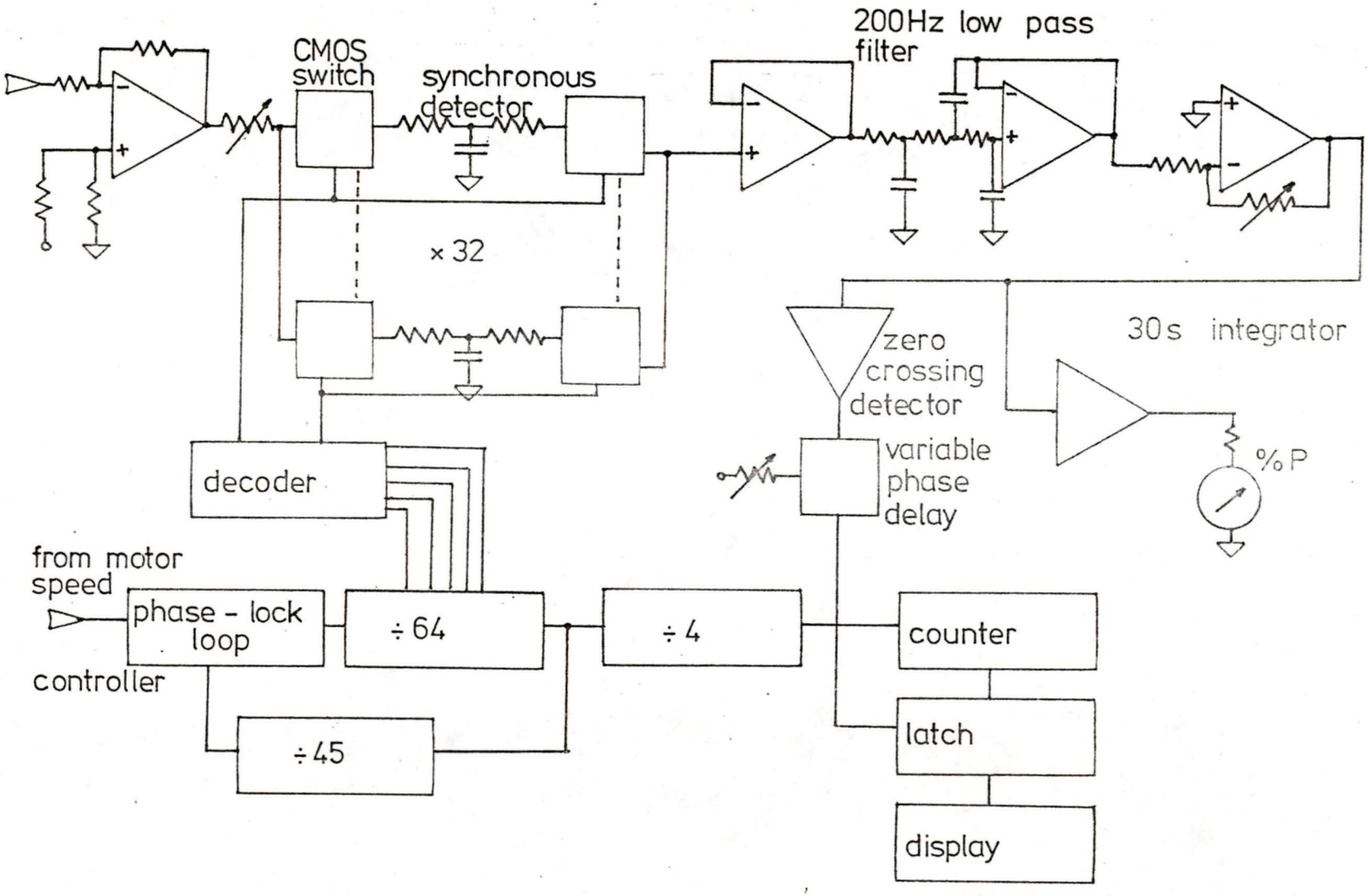
CMOS switch
synchronous detector
200Hz low pass filter
× 32
30s integrator
zero crossing detector
variable phase delay
%P
decoder
from motor speed
phase - lock loop
controller
÷ 64
÷ 4
÷ 45
counter
latch
display

VITA

Surname: ECCLES Given Names: MICHAEL JOHN

Place of Birth: CARDIFF, WALES Date of Birth: 11 July, 1944

Educational Institutions Attended, with Dates of Entering and Leaving:

LIVERPOOL UNIVERSITY, ENGLAND 1962 to 1968

UNIVERSITY OF VICTORIA, B.C. 1976 to 1978

Degrees awarded:

B. Eng. (Honours) 1965 Liverpool University, England

Ph.D. 1969 Liverpool University, England

Awards:

University of Victoria Fellowship, 1976/7, 1977/8

Publications:

Eccles, M.J., and Craggs, J.D. (1967), Electronics Letters, 3, 146.

Eccles, M., Prasad, A.N., and Craggs, J.D. (1967) Electronics Letters, 3, 410.

Eccles, M.J., O'Neill, B.C., and Craggs, J.D. (1970), J. Phys. B: Atom. Molec. Phys., 3, 1724.

Eccles, M. and Kapuskar, W. (1970), Hewlett Packard Analytical Advances, 3, 14.

PARTIAL COPYRIGHT LICENSE

I hereby grant the right to lend my thesis (the title of which is shown below) to users of the University of Victoria Library, and to make single copies only for such users or in response to a request from the library of any other university, or similar institution, on its behalf or for one of its users. I further agree that permission for extensive copying of this thesis for scholarly purposes may be granted by me or a member of the University designated by me. It is understood that copying or publication of this thesis for financial gain shall not be allowed without my written permission.

Title of Thesis

OPTICAL POLARIMETRY OF FIVE STARS

Author [redacted]

Michael John ECCLES

10th April, 1979